EFFECTS OF INLET GEOMETRIES ON FLOW RECIRCULATION IN AN AXIAL-FLOW PUMP

A Thesis

by

KENAN ALPAN

Submitted to the Graduate College of
Texas A&M University
in partial fulfillment of the requirements for the degree of

MASTER OF SCIENCE

December 1984

Major Subject: Mechanical Engineering

EFFECTS OF INLET GEOMETRIES ON FLOW RECIRCULATION

IN AN AXIAL-FLOW PUMP

A Thesis

by

KENAN ALPAN

Approved as to style and content by:

Dr. Peter Jenkins
(Chairman of Committee)

Dr. Gerald Morrison
(Member)

Dr. Aydin Akgerman
(Member)

Dr. A.B. Alter
(Interim Head of Department)

December 1984

ABSTRACT

Effects of Inlet Geometries on Flow Recirculation
in an Axial-Flow Pump. (December 1984)
Kenan Alpan, B.S., Texas A&M University
Chairman of Advisory Committee: Dr. Peter Jenkins

Experiments have been carried out in order to determine the effects of different inlet geometries on the onset of suction recirculation and its associated power consumption in axial flow pumps.

The experiments were conducted with water on an axial-flow pump which was originally designed as an F-15 jet's fuel pump. Tests were performed at two different speeds with flowrates ranging from fully open to shutoff.

In addition to power, velocity and pressure measurements were taken at different suction sections with varied flowrates to obtain the pumps' characteristic curves. Variations of the pump critical flowrate with different impeller inlet areas, suction piping and inlet guide vanes were determined. The results and test methods were compared with similar investigations as well as recently developed theories. Modifications to experimental set-up and possible future studies and recommendations are discussed.

DEDICATION

I dedicate this work

to

my parents

DR. SADRETTİN and MARY ALPAN

for their love, support, encouragement and companionship.

ACKNOWLEDGEMENTS

I would like to gratefully acknowledge all of those who have contributed and have made this research possible:

I thank Dr. William Peng and Dr. Peter Jenkins for serving alternately as my Advisory Committee Chairman, for their leadership, and for providing me with very valuable information, guidance, encouragement and financial support.

I thank Dr. Gerald Morrison and Dr. Aydın Akgerman for their interest, recommendations, and for the honor of having them on my advisory committee.

I would also like to extend my appreciation and gratitude to the Turbomachinery Lab and its staff, primarily to Mr. Eddie Denk and Mr. David Hassinger for providing me with valuable help, advice and knowledge.

I finally would like to acknowledge my colleagues, Mr. Tony Prince and Mr. Ketan Sheth, with whom I had the pleasure of working and learning.

TABLE OF CONTENTS

TABLE OF CONTENTS

(Continued)

LIST OF TABLES

LIST OF FIGURES

LIST OF FIGURES

(Continued)

LIST OF FIGURES

(Continued)

LIST OF FIGURES

(Continued)

NOMENCLATURE

A	Area (in^2)
C	Conversion and discharge coefficients and theoretical correction factor
C_m	Moment coefficient
D	Diameter (impeller, pipe) (in)
D_h	Hydraulic diameter (in)
D_n	Dimensionless parameters
F	Function
H	Pump head (ft)
I	Principal meter constant
K	Flow constant
L	Length (ft)
M	Mass (lb_m)
N	Pump rotational speed (rpm)
N_s	Pump synchronous speed (rpm)
NPSH	Net Positive Suction Head (ft)
P	Pump power consumption (Hp)
P_{av}	Average circumferential pressure (psi)
P_b	Bench wattmeter power reading (W)
P_d	Discharge pressure (psi)
P_f	Reference static pressure (psi)
P_{in}	Total input power (W)
P_p	Panel wattmeter power reading (W)
P_r	Power loss due to suction recirculation (Hp)

NOMENCLATURE
(Continued)

P_s Static pressure (psi)

P_{sh} Input shaft power (Hp)

P_{suc} Suction pressure (psi)

P_t Total stagnation pressure (psi)

Q Flowrate (gpm)

Q_{cr} Pump critical flowrate (gpm)

Q_o Pump design flowrate (gpm)

Q_r Section critical flowrate (gpm)

R Suction pipe radius (in)

Re Reynolds number

S Motor slip (%) and wetted perimeter (in)

T Torque (lb.in)

U Impeller peripheral velocity (fps)

V_a Axial velocity (fps)

V_t Tangential velocity (fps)

X Location of inlet pressure taps (in)

d Orifice diameter (in)

f Supply frequency (Hz)

g Gravitational constant (ft/sec^2)

h Height of conical cover (in)

h_w Orifice differential pressure (psi)

i Angle of incidence (deg)

m Independent dimensions

NOMENCLATURE
(Continued)

n	Number of variables and power and velocity equation exponent
p	Number of motor poles
r_h	Hydraulic radius (in)
r_i	Impeller radius (in)
r_t	Geometric radius (in)
t	Time (sec)
u	Theoretical true velocity (fps)
v	Local flow velocity (fps)
$\bar{v}$	Average velocity (fps)
α	Angle of inclination (deg)
β	Diameter ratio, flow/blade angles
ε	Calibration correction factor
η	Efficiency (%)
η_m	Motor efficiency (%)
η_o	Overall efficiency (%)
ϕ	Flow coefficient
γ	Specific weight (lb_m/ft_3)
μ	Absolute viscosity (lb_f-sec/ft^2)
ν	Kinematic viscosity (ft^2/sec)
ω	Angular velocity (rad/sec)
Π	Through flow power coefficient
Π_1	Capacity coefficient

NOMENCLATURE
(Continued)

Π_2	Head coefficient
Π_3	Shutoff power coefficient
Π_4	Reynolds number coefficient
ρ	Fluid density (lb_m/ft^3)
θ	Circumferential pressure tap location (deg)
Amp	Amperes
Atm	Atmosphere
fps	Foot per second
gpm	Gallons per minute
Hp	Horsepower
Hz	Hertz
in.	Inches
psi	Pounds per square inch
rpm	Revolutions per minute
V	Volts
W	Watts

CHAPTER I. INTRODUCTION

Displacement of various liquids has been an important aspect of our lives throughout history. Nowadays we have machines called pumps to perform this difficult task for us. There exists many variations in pump design: mainly the centrifugal, axial, mixed and positive displacement types. Pumps find wide applications, especially in the agricultural and industrial environments, and the very existence of the industry depends on them.

The goal of any pump is to achieve a certain desired head under various operating conditions, i.e., the addition of energy to the fluid. The manufacturer always supplies the user with the pump performance and system curves where the corresponding pressure and flowrate ranges are indicated, the point corresponding to the maximum or best efficiency occurs at the vicinity of the design point. Unfortunately, pumps quite often have to operate at flowrates other than the design one in order to satisfy system requirements. The intersection point of the performance and system curves is defined as the pump operating point. The most practical means of achieving various required flowrates is by throttling the discharge valve. This changes the friction losses of the fluid which causes the alteration of the system curve resulting in a different flowrate.

As the flowrate is decreased, it becomes apparent that at a certain capacity, the flow starts reversing itself from the impeller

---

This thesis follows the style of the Journal of Fluids Engineering.

towards the inlet duct at the outer periphery of the pipe. This flow reversal occurring at the suction or discharge tips of the impeller vanes is referred to as flow recirculation. It is always accompanied by a swirling flow called prerotation. The case where the swirl and impeller have the same sense of rotation is regarded as positive prerotation. With the start of prerotation, the flow becomes a complicated three-dimensional flow.

The flowrate where reverse flow is initiated is known as the "section critical flowrate" for any section upstream of the impeller under investigation. As flowrate is reduced, the recirculation increases its intensity and propagates upstream until it reaches a maximum at shut-off conditions. The flowrate at which the reverse flow initiates at the impeller tips is our primary concern and is called the "pump critical flowrate."

Recirculation carries some portion of the energy created by the impeller back into the suction line through the outer periphery of the pipe while the fluid flow is directed back to the impeller at the core of the pipe. This energy dissipation is highly undesirable and detrimental to the pump's operation and life. Most pump problems at low flow rates are attributed to this phenomena. Recirculation and hydraulic losses are the two major reasons for the performance curve being of a parabolic nature instead of a linear one as it would be expected from theory. Unfortunately, it is impossible to avoid recirculation completely except for the ranges around the design point, so our efforts were concentrated on reducing it to an allowable minimum.

When the pump is operated at flows lower than the critical, it is observed that the input power required increases with a drop in efficiency. Therefore, it is most beneficial to delay the start of recirculation, especially if high heads and a stable pump performance is desired. The main objectives of the present study can be stated as:

1. Determining the effects of various inlet geometries on suction recirculation and pump performance.
2. Determining input power consumption solely due to recirculation and developing means for its reduction and prediction.
3. Determining the velocity, pressure distributions and critical flow rates at three different suction sections in order to develop the flow pattern and to determine the effects of recirculation.
4. Develop the performance curves for the pump.
5. Determine the effects of speed variations on recirculation.
6. Correlate shaft power and critical flowrates with pump inlet geometries by using nondimensional parameters.
7. To compare results with previous studies performed with straight piping and standard inlet conditions.
8. Check validity of proposed analytical approaches by using experimental results.
9. To determine and suggest the best recirculation delaying technique or combination of techniques for industrial and commercial usage.

In recent years, recirculation has received great attention from both academic and industrial circles. Pump users, designers and researchers have likewise brought up and discussed their problems associated with recirculation in papers, articles, symposiums and meetings.

Extensive research still needs to be carried out in order to achieve a comprehensive understanding of the phenomena. It is hoped that this study will serve as one of the links in a chain of studies addressing the subject and provide a basis for future studies.

To promote a better understanding of recirculation among the pump designers and users, and to aid future investigators, a concise literature survey has been conducted and presented in the next chapter.

CHAPTER II. LITERATURE SURVEY

2.1 Introduction

Even though there have been quite a few studies performed on recirculation, most of them have been for centrifugal pumps while only a few for axial and mixed-flow pumps [1-6]. Reverse flow studies are performed at the suction and discharge sides of various pumps in order to identify the reverse flow characteristics and to determine its effects on the overall machine performance. From these studies it is confirmed that recirculation exists at both the suction and discharge sides of the pumps.

Different aspects of recirculation such as its determination, mechanism, causes, means to delay and predict its occurrence, and the problems associated with it will be discussed in the following sections.

2.2 Backflow Analysis Techniques and Instrumentation

A variety of experimental methods have been used in previous studies of pump recirculation. Visual observations have been possible by utilizing transparent plating and piping [1,2,3,7,8,9,10,11,12,13] together with electronic stroboscopes [2,7,8,12], strings or wool tufts [1,2,11,13], oil films [8], and hydrogen bubbles [9,10]. Even though visual observations give us a good insight into the problem, they only provide guidance to the solution.

In most of the investigations, the pressure and velocity measurements were performed by pitot-probes, differential pressure transducers, manometers and piezometers. In some instances the velocities were recorded by a laser doppler anemometer.

2.3 Flow Characteristics

Results of all studies agree that at low flowrates the velocity and pressure profiles are asymmetric in form. The degree of asymmetry further increases with the gradual decrease of the flowrate.

Of the three velocity components, the magnitude of the tangential velocity is zero at the pipe axis and it increases rapidly towards the pipe periphery as the flowrate is decreased. The axial component is referred to as positive when traveling towards the impeller, and negative when progressing upstream. As the flowrate is decreased beyond the critical point the negative flow increases in proportion. The radial velocity is very minimal but gains significance at very low flows.

The axial and tangential velocity profiles are observed to be the same along the suction pipe. The general profile does not vary with the pump speed, it follows the law of similarity [14,15]. These authors indicate that at low discharges, the reverse flow may reach up to seven pipe diameters from the inlet plane.

The swirling character of the reverse flow sets up an asymmetric pressure distribution in the suction pipe of both axial and centrifugal pumps [2,14,15,16,17,18]. The static pressure varies circumferentially at the pipe wall, peaks and depressions are noted at certain

angles. Sen [17] determined these extremes to be 180 degrees apart. Schiavello [16] attributed the asymmetry to the impeller geometry and volute.

At high flowrates the pressure values in the pipe upstream are higher than the ones at the impeller plane, due to the wall friction losses. However, when the pump is operating at low flow, the swirling reverse flow is initiated and the trend is reversed. It is recommended that in determining pressure-rise across the pump, the suction pressures should be taken at far upstream distance and the friction losses accounted for.

2.4 Causes and Mechanisms of Backflow

The reason for the occurrence of recirculation is still somewhat ambiguous. Even though there have been several proposals, it is yet to be seen for one theory to gain wide acceptance and support. As it is in most pump related topics, the first principal investigator of recirculation was Stepanoff [19]. He explained the formation of recirculation by his "Least Resistance Principle" where the fluid is assumed to follow a path in such a way that it encounters the minimum resistance on its way to the impeller channel with the flow angle of attack approaching the vane angle.

Peck [7] was one of the early investigators to detect recirculation. He based its formation on the oncoming water striking the forward side of the vane tips and creating a mean pressure differential across these tips. Due to the uneven loading powerful back eddies are

formed behind the vane tips, causing the water to rotate into the suction.

Stepanoff and Peck were followed by several authors who based the cause on one specific or a combination of factors. A few of them indicated the increase of the flow angle of attack as the main reason [2,3,5,20,21], while others saw the geometrical design parameters more influential [1,4,22,23]. The main parameters would be the inlet pipe configuration, number of blades, impeller eye diameter, blade camber variation, wear ring clearance, and the impeller-volute gap. The pressure gradient created by the dynamic head exceeding the centrifugal head in the impeller is also cited as one of the main causes [18,24]. A final group of researchers have concluded that reverse flow is initiated by a boundary layer separation occurring at the leading edge due to a combination of the factors mentioned above [8, 14,16,25,26].

Schiavello and Sen offer a thorough analysis for the inception of recirculation [26]. He suggests that if the delivery is decreased, the incoming flow reaches a high incidence angle causing high blade loading on the leading edge of the suction side. At a certain flow-rate, the stalling incidence angle is reached and local separation starts. As the flow is further reduced and the back pressure increased, a reverse flow arises immediately for centrifugal pumps and with a delay for axial and mixed flow pumps. Prerotation is induced by the reverse flow through the action of the viscous shearing forces, and immediately follows backflow. Toyokura [18] confirmed the responsibility of the flow separation causing backflow with an axial-flow

pump. An increased angle of incidence and a high radial velocity component force the fluid to concentrate at the pressure side of the blade at the impeller tip. Fluid "slip" is seen as a contributor to the velocity effect. The high pressure zone moves to the inner part of the flow passage. The fluid at the blade tip undergoes an increase in relative velocity and then separates from the blade causing a pressure drop at the blade tip. The high pressure zone, still present in the blade passage, forces the fluid to flow out reversely.

Blade loading critically affects separation by creating secondary flows which transport low momentum fluid from the impeller hub to the tip. This fluid accumulates in the tip boundary layer which consequently becomes more susceptible to separation [16,17,26]. The flow angle of attack (incidence), "i", is an essential parameter in the occurrence of separation. The smaller "i" is, the closer the flow entry conditions are to a "shockless" entry where the blade and flow angles are equal. It is worthwhile to add that pumps with low Net Positive Suction Head Required (NPSHR) values, and double suction pumps are more susceptible to recirculation [22,27].

2.5 Associated Problems

The pump problems attributed to suction and discharge recirculation were gathered from a wide variety of literature, and they can be itemized as follows:

a) erosion of the impeller vanes at both sides,

b) axial thrust to the shaft causing damage to the bearing,

c) cracking or failure of the impeller shroud,

d) permanent damage to the stationary vanes,

e) hydraulic surging on the suction side,

f) intense vortices with high velocities resulting with high wall static pressures at the pump inlet,

g) formation of intense cavitation,

h) severe pressure pulsations and noise,

i) loss of energy with fluid flow back into suction,

j) instabilities of the head characteristics at shut-off,

k) severe drop in efficiency,

l) negative head gradient at low deliveries,

m) operating range of pump is decreased,

n) excessive vibration levels, and

o) mechanical seal damage.

Despite elaborate research in the field of cavitation no study has been done to determine its interaction with recirculation. It is believed that they both contribute to the blade erosion. Homogenous liquids such as water are more susceptible to vaporize and induce cavitation. When the local pressures become lower then the pumped liquid's vapor pressure, vapor bubbles are formed and thus cavitation initiated. Recirculation is presumed to be the cause of low pressures, and by impinging on the blades the bubbles cause erosion.

Modifying the impeller and the inlet geometry should most likely retard the onset of recirculation and enhance stability. Increasing the blade camber angle with the solidity [2,18], equalizing hub to tip loading, and lowering the incidence angle [26] all proved to be very

effective in delaying the occurrence of reverse flow and reduced associated problems.

2.6 Inlet Geometries

Modifying the pump inlet geometry is proven to be one of the most effective ways to delay recirculation. Some authors have gone by redesigning the impeller, while others by installing various devices at the pump inlet.

Schweiger [23] extended the blade edge of a centrifugal impeller into the suction nozzle to obtain high and stable heads. Then he perpendicularized the impeller edge with the shaft axis to claim all the power lost due to recirculation when the edge was parallel. Inlet flow symmetry and critical flowrate delay is enhanced with the matching of the impeller/volute characteristics at the pump operating point [16,17].

Some investigators installed flow straighteners or inlet guide vanes at the pump inlet [2-4,7,23]. Schweiger tested straighteners with four and eight blades and concludes that the four blade vane drew less power with high heads, while the eight blade design caused extra friction losses. The usage of inlet devices such as conical impeller covers, anti-stall rings and hollow circular plates also gave improved results [1,6,28,29]. Throttling the impeller eye proved very effective, but adversely affected pump performance at high flows. Besides reducing the critical flowrate, these devices recovered most of the power lost due to recirculation. The anti-stall rings apparently

broke the recirculatory flow yielding a higher operating range, but no significant improvements were made in delaying recirculation.

Changing the inlet piping is another alternative to suppress recirculation. Murakami tested piping with 45 and 90 degree elbows [30]. It is observed that at low flowrates the reverse flow proceeds upstream of the 45 degree elbow, creating an asymmetric velocity profile. However, the flow does not pass through the 90 degree elbow, leaving the flow axisymmetric at elbow upstream. By inducing secondary flow, the elbows affect the inlet circumferential pressure distribution.

The most recent addition to the inlet devices is the backflow recirculator [21]. This device collects any swirling backflow from the impeller inlet, deswirls it and returns it to the mainstream at pipe upstream. The recirculator is stationary, does not block the inlet, and if correctly designed does not adversely affect the pump performance over the entire flow range. Test results prove to be very favorable, and it seems like this is the best inlet geometry so far.

2.7 Analytical Predictions

The two parameters that have been approached analytically are the critical flowrate, Q_{cr} and the power loss due to recirculation, P_r. Experimentally Q_{cr} is found to be occurring at a range of 40 to 85% of the nominal flowrate. This value depends on the pump itself, but a median of 50 to 60 % is usually cited. Experimentally the critical flow is widely determined by observing string reversals and by measuring suction pressure at different sections. When the reverse flow

propagates upstream strings attached to the pipe wall reverse their directions and the suction pressures rapidly increase due to the swirl. When pressures are plotted a discontinuity point between the two pressure zones appear, and it is designated as the critical flowrate. From the trend of the section critical flowrates, the pump critical flowrate can easily be found.

A means of knowing the pump lower end operating limit beforehand would be of great value and contribution. Fraser [31] proposes the suction specific speed and the ratio of hub to tip diameters as the governing parameters for the prediction of backflow occurrence. A curve relating these two parameters based on empirically derived formulas would be used to select and apply the pump. This approach has been proven not to be very accurate, but a fairly good approximation [13]. In this recent study the critical flowrate was tried to be determined from the input power, but results in a high uncertainty.

When the pump is operating under recirculatory conditions, a portion of the input power is lost to the reversing flow. This loss increases as the flowrates approach shutoff conditions, and it can constitute up to 30% of the input power in some cases. From the energy saving and financial viewpoint, it would be critical to know the loss for various pumps. Recently, Tuzon [32] proposed a formula to predict it, the results of this study will be applied to his formula, and results included in Chapter 5.

Experimentally and analytically there still is a lot more to be done in order to achieve a comprehensive understanding of this complex subject.

CHAPTER III. EXPERIMENTAL APPARATUS

3.1 Introduction

The experiments were carried out at the Turbomachinery Laboratory located at the Research Annex of Texas A&M University. Besides a few minor changes, the test rig used was the same one utilized by Prince [1]. Figures 1 and 2 show a general view and a schematic diagram of the test facility respectively.

3.2 Test Pump

The pump used for all tests was originally designed and manufactured as an aircraft fuel booster pump by TRW, Inc. (Fig. 3). This pump was designed to operate within the fuel system of the F-15 fighter jet which is manufactured by the McDonnel Douglas Corporation. The pump actually is a motor-pump set which is fitted on the same shaft. The motor, rated at 2.8 hp is a squirrel cage, eight pole, Y connected induction machine and must be supplied from a three phase, 220 volt, AC source at a rated frequency of 400 Hz.

The pump impeller has two stages. The first one is of the axial (diagonal) flow type having three blades, each inclined 40 degrees with the shaft axis (horizontal) and a tip-to-tip diameter of three inches (Fig. 4). This stage is used during normal mode of operation while the radial stage in the back gains significance when the aircraft is subjected to negative accelerations or flying at inverted altitudes. In the present study, the radial stage is sealed from the

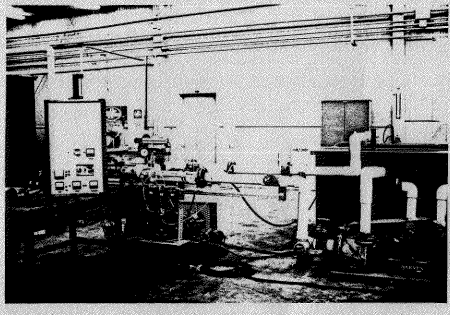

Figure 1. General view of test facility.

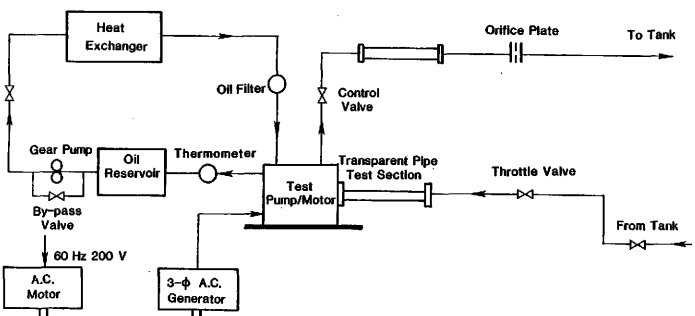

Figure 2. Schematic diagram of test facility.

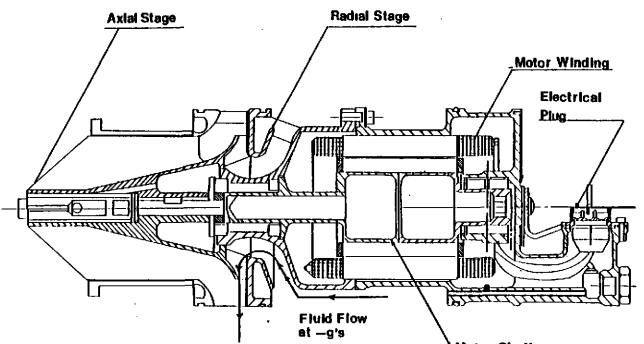

Figure 3. Sectional view of test pump.

Figure 4. View of impeller axial stage.

main flow passage (Fig. 5), only the axial stage is employed for pumping operation. The aluminum casing of the impeller and the pump motor is shown in Figure 6.

3.3 Power Supply

The power required by the pump is provided through a generator manufactured by Bendix. It will supply 25 Amp current at a frequency of 400 Hz and 208 volts line to line, at a rated speed of 4000 rpm. The intensity of the current, the frequency and the supply voltage are all proportional to the speed which the generator is driven at. A synchronous motor rated at 1725 rpm and 10 hp is the prime mover. It is coupled with the generator by a set of pulleys and V-belts to produce the generator output at a lower frequency of 278 Hz as well as the rated frequency of 400 Hz. The power supply system is schematically shown in Figure 7.

The generator output was connected to a carbon pile regulator while three 25 Ampere fuses were installed before the motor-pump set for motor overload protection. The power was transmitted to the pump-motor set by a five pin Cannon connector. Power, current and voltage readings were made possible by a set of panel meters. The wattmeters which were normally operated at 60 Hz had to be recalibrated at 278 and 400 Hz by means of bench wattmeters. A different wattmeter configuration was used with each of the running speeds and the selection of the appropriate configuration was made possible through a set of switches. The two different wattmeter configurations and the detailed

Figure 5. View of impeller radial stage.

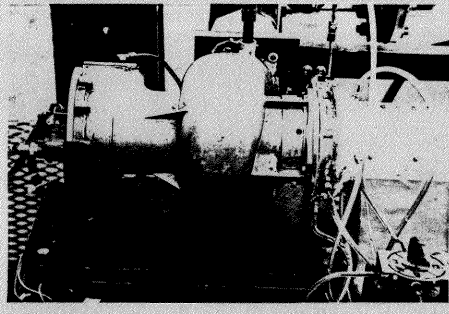

Figure 6. View of pump casing.

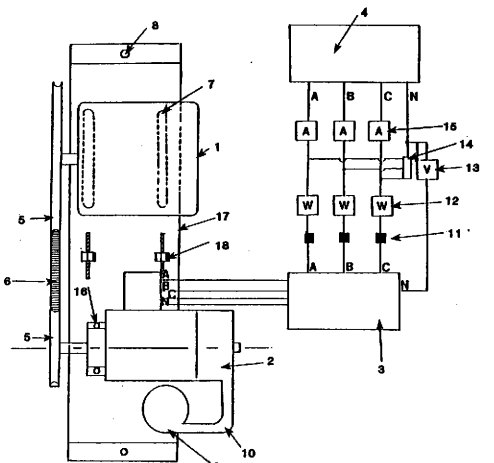

Figure 7. Schematic diagram of power supply.

calibration setup are presented in Appendix A. All meters were mounted on a control box, which also housed the regulator and the fuse box. The power system setup is shown in Figure 8.

3.4 Hydraulic Loop

A closed water loop was constructed for continuous operation. The 700 gallon tank and the pump were connected by 3 inch dia. PVC pipes of schedule 40. The supply tank was equipped with baffles, a drainage pipe and a flow strainer. Two gate valves were installed at the suction and discharge PVC pipes to throttle the flow. Plexiglass pipes were installed at the pump inlet and outlet for flow visualization and copper tubular flow straighteners were placed just upstream of these sections. The general view and the schematic diagram of the hydraulic loop can be seen in Figures 9 and 10 respectively.

The pump and the suction plexiglass were adjoined together by means of an aluminum spacer. Several holes were drilled at the inlet piping for pressure taps and positioning of the pitot probe, various inlet geometries and strings. Their exact locations will be described in the latter sections. Two other pressure taps were used, one at discharge and the other at far upstream, for discharge and static head measurements. Epoxy glue coated 1/8 inch copper tubes were inserted into all taps for accurate readings and to prevent water leaks.

3.5 Lubricating and Cooling System

Since the pump is fully submerged in the fuel tank aboard the aircraft, the jet fuel acts both as a lubricant and a coolant besides

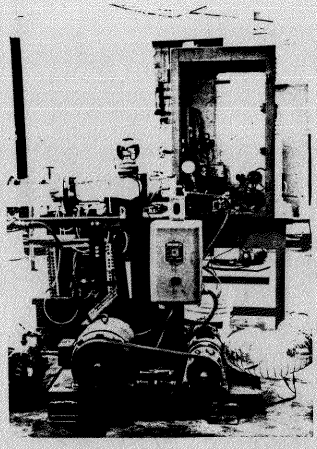

Figure 8. View of power supply.

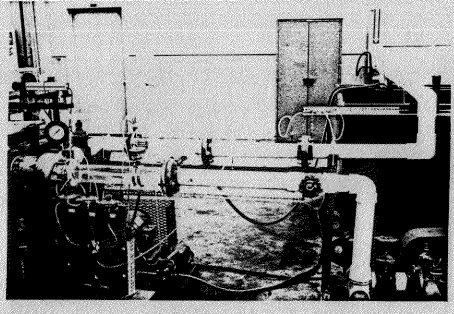

Figure 9. View of the hydraulic loop.

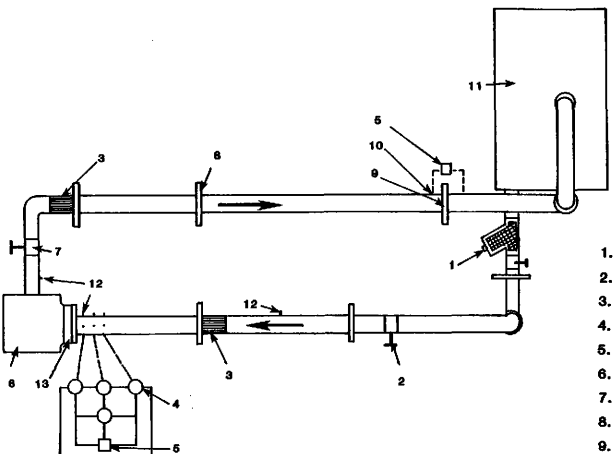

1. Strainer
2. Inlet valve
3. Flow straightener
4. 5 port valve
5. Pressure transducer
6. Motor/pump set
7. Discharge valve
8. Plexiglass pipe
9. Orifice plate
10. D & 1/2D taps
11. Supply tank
12. Pressure taps
13. Aluminum spacer

Figure 10. Schematic diagram of hydraulic loop.

being the pumped medium during the normal mode of operation. In our study, water is used as the pumped medium. The danger that it would bear upon the motor coils necessitated our use of another medium for lubricating and cooling purposes. Because of being abundant, economic and widely applied, hydraulic 10W oil was chosen. Both the water and the oil had to be circulated through the pump, so a means of separation needed to be devised. This was achieved by inserting a lip seal in the radial impeller, but after some usage it failed and mixing occurred. The problem was remedied for good by mounting two single lip seals back to back.

Because of its availability, an automotive air conditioning condenser was used as the heat exchanger for the cooling/lubricating system. The pressure loss due to friction in the heat exchanger, the oil lines and the oil filter was determined to be approximately 60 psi. A rotary gear pump with a bronze casing made by Oberdofer was chosen to overcome this pressure drop. The 1000R model had a bypass valve making flow and head control possible. The oil pump assembly may be seen in Figure 11. The heat exchanger was immersed in the water tank which acted as a cooling medium. By discharging the returning flow close to the heat exchanger the heat removal process was enhanced. The oil was supplied from a five gallon sump and circulated through the heat exchanger, a 25 micron oil filter and the test pump. The oil line was made out of 1/2 inch hydraulic hose and the schematic diagram of the whole cooling, lubricating loop is given in Figure 12.

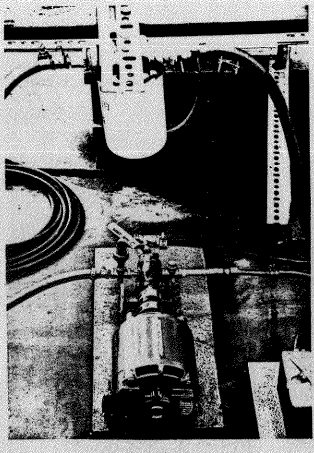

Figure 11. View of lubricating/cooling system.

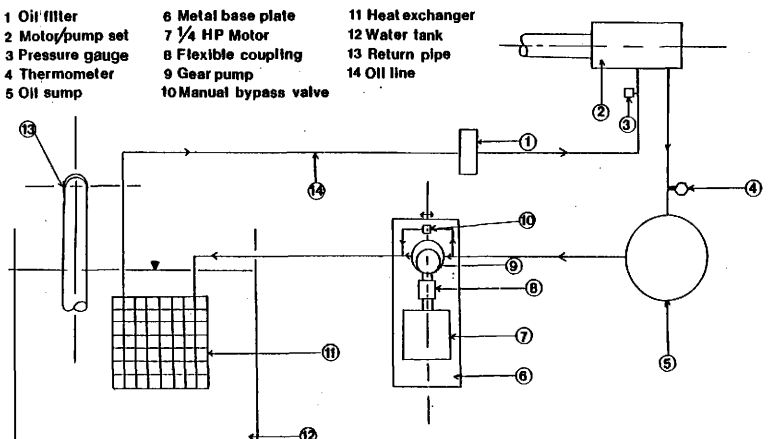

Figure 12. Schematic diagram of the lubricating/cooling system.

Oil was injected into the pump through a threaded fitting located at the rear portion of the pump. The oil flow path and the minor modifications such as the installment of the double lip seal are shown in Figure 13. After accumulating in the inner pump housing, the oil is returned to the reservoir via copper and plastic tubing. The oil pressure and temperature were monitored by means of a pressure gauge at the motor inlet and a thermometer at the outlet respectively. The inlet and discharge oil lines and the monitoring devices are shown in Figure 14. It is worthwhile to note that this system served satisfactorily throughout all testing.

3.6 Inlet Geometries

Since our main goal was to delay the onset of suction recirculation it was important for us to see the effects of various inlet geometries on this phenomena. Impeller cover cones were used in order to restrict the impeller inlet area, while a U-pipe configuration was used instead of the plexiglass to see the effects of creating a resistance to the backflow by introducing the elbows. Along with the clear plexiglass pipe conical, cross and channel vanes were used. With the conical guide vane it was intended to see the effects of increasing the flow velocity at the outer radius and by installing box, cruciform vanes it was hoped to see improvement by preventing the prerotation, which always accompanies the recirculation.

The cones were made out of a hardening epoxy resin, Epon 828 of Shell Chemicals and a curing agent, VZ40, the mixture was poured into a mold and cooled. The 1/8 inch thick cones were designed to have the

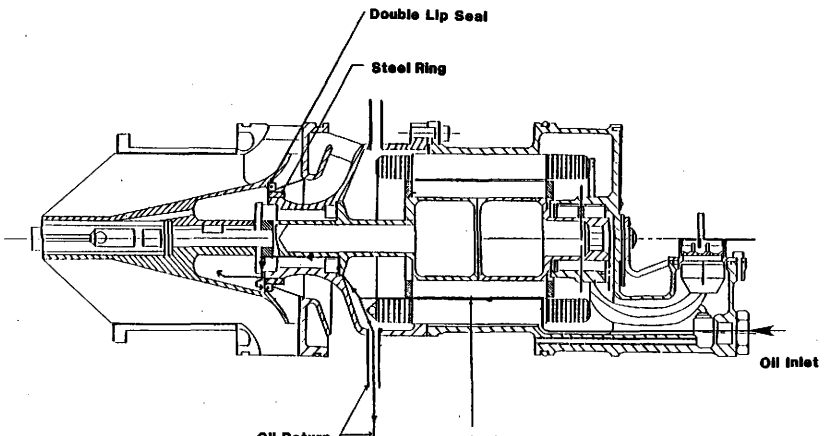

Figure 13. Pump modifications for water/oil separation.

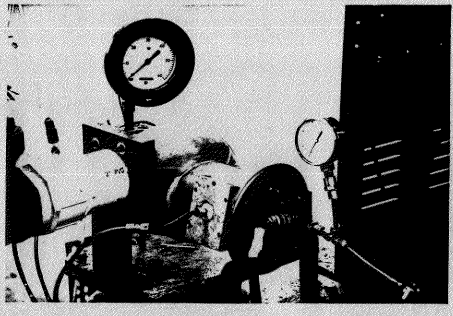

Figure 14. View of oil inlet and return from pump.

same shape as the impeller leading edge but with different frustrum heights. The conical impeller covers are shown in Figure 15. The cones were mounted from their bases to the inner pump housing by means of set screws. Drawings of the mold and the mounting are presented in Appendix A. The pump inlet geometry with a cone mounted, the impeller and the pressure tap sections are presented in Figure 16.

The U-pipe configuration was made from 3 inch PVC pipes, four elbows and two flanges. Two sets of pressure taps were drilled on the side closer to the pump inlet, and the assembly was supported by a 4x4 wooden block for stability. The inlet guide vanes were all made out of thin sheets of stainless steel. All geometries except for the cones are presented in Figure 17 with their actual dimensions at different views.

3.7 Instrumentation

The instrumentations employed in the present study are mainly to make the measurements of pressure, flowrate, flow velocity and motor power.

All pressure readings were made possible by the use of multi-range Validyne pressure transducers. Carrier demodulators transformed the transducer output signals to DC voltages which were digitally displayed on a voltmeter. Pressure differentials across the pump and the orifice plate as well as suction pressures were all recorded by this means. Before each test, the transducers were calibrated, the

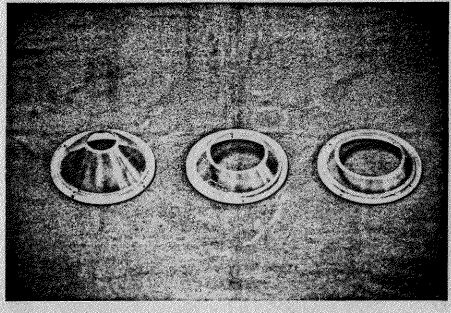

Figure 15. View of conical impeller covers.

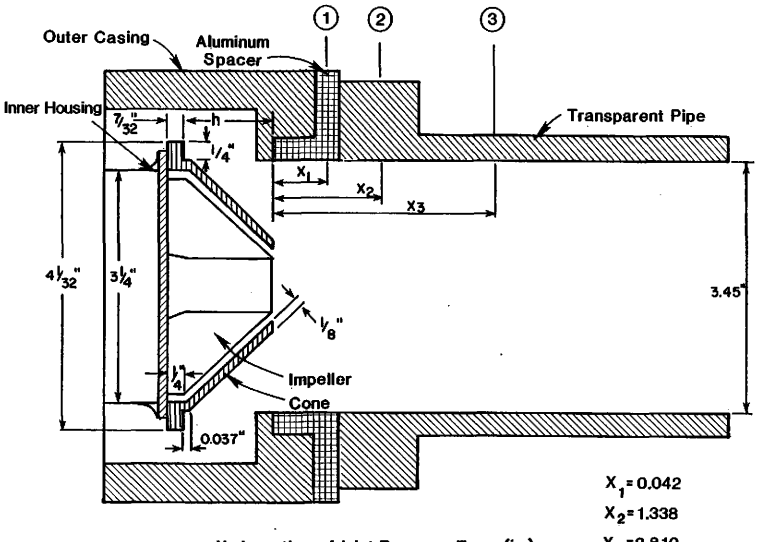

Figure 16. Pump inlet geometry and pressure tap locations.

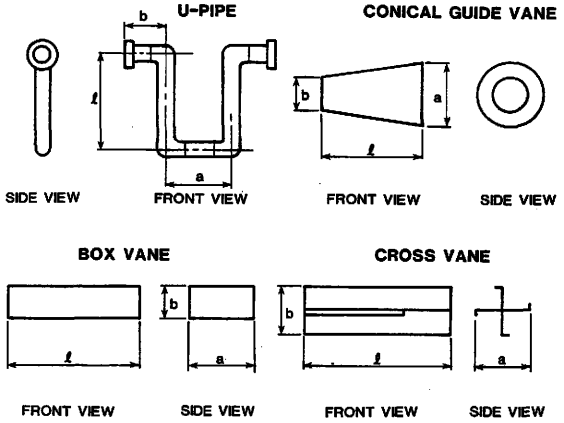

INLET GEOMETRY	ℓ (in.)	a (in.)	b (in.)
U-PIPE	28.00	10.44	5.76
CONICAL GUIDE VANE	4.00	2.20	1.68
BOX VANE	10.00	3.25	1.25
CROSS VANE	10.00	3.25	3.25

Figure 17. Dimensions and diagrams of inlet geometries.

high range ones with a dead weight tester and the low range ones with a mercury manometer.

A stainless steel square edge orifice plate was installed at the discharge portion of the hydraulic loop. Flowrate calculations were based upon the recorded pressure differentials across this plate. All suction pressures were made available by the use of 1/8 inch plastic tubing and four 5-way ball valves. As shown in Figure 18, all four pressure taps in each of the three suction sections were connected to the inlet ports of the corresponding valves by the plastic tubing. The output ports of the three valves and the upstream pressure tap were all connected to the inlet of the fourth valve, which acted as the heart of the "pressure operation." The output of this last valve was connected to the transducer and the readings were made with respect to atmosphere. This monitoring system provides a convenient way to select the desired pressure measurement. The suction area with the pressure controls during operation is shown in Figure 19. A pressure gauge was also installed at the immediate discharge of the pump in order to monitor the discharge pressure.

Flow velocity measurements were performed using a five hole prism shaped 1/8 inch pitot probe manufactured by United Sensor. The total pressure at any point in the flow is measured by the centrally located hole when the two lateral side hole pressures are equalized (i.e., central hole in alignment with flow direction). The flow static pressures were recorded at exactly 90° from the point of total pressure

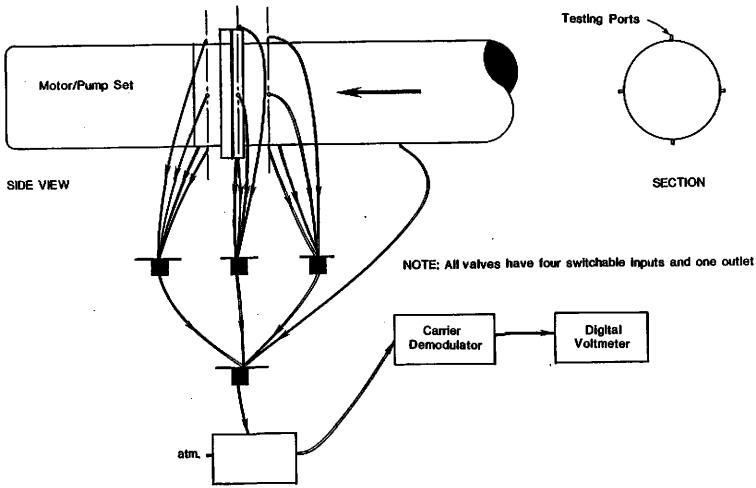

Figure 18. Schematic diagram of inlet pressure monitoring system.

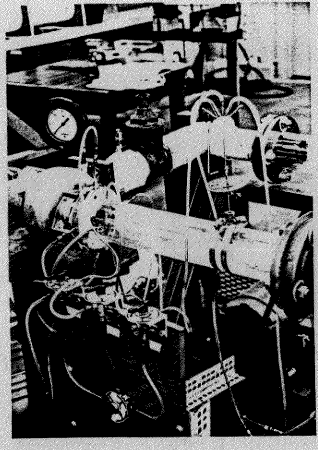

Figure 19. View of pump inlet test section.

measurement. The pressure readings were made with transducers which were connected to the outlet tips of the probe by plastic tubing. These recorded values were theoretically converted into velocity terms. The angle measurements were achieved through the use of a simple protractor and a reference point on the probe mount. The probes' vertical motion was made possible by this mount and a special water-tight guide directed it into the test section. This whole assembly is shown in Figure 20. A calibration curve was developed for the pitot probe at far upstream distance, where the flow is surely free of recirculation. All data was corrected with the use of this curve.

The electrical power input were read from panel wattmeters which were calibrated against bench wattmeters while the input voltages and currents were monitored by panel voltmeters and ammeters. All other relevant devices and instruments utilized during testing were included in the preceding sections.

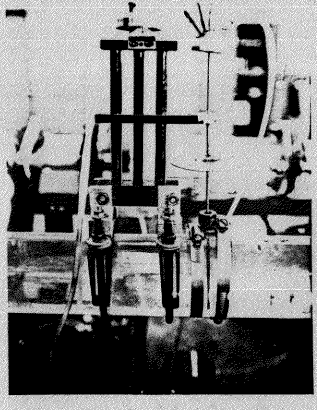

Figure 20. View of pitot probe and its mount.

CHAPTER IV. EXPERIMENTAL STUDIES

4.1 Introduction

With this chapter it is intended to give the reader an overview of the whole experimental procedure. A few derivations and calculations relevant to the data analysis will be presented first, then it will be followed by a thorough explanation of the test procedure. Finally, the calculations and results of the main pump characteristics, such as the shaft power, head and overall efficiency will be presented and discussed.

4.2 Dimensionless Coefficients

With the aid of dimensional analysis it is possible to determine the relevant dimensionless constants, which can facilitate drawing conclusions and comparing pump behavior among geometrically and kinematically similar pumps. The most convenient procedure to obtain these dimensionless parameters is based on the "Buckingham Π" theorem, and it can be stated as follows: the number of dimensionless products representing a physical phenomena can be deduced from "n" variable parameters and "m" independent dimensions arranged as (n-m). Generally in turbomachinery practice 6 to 8 variables (n) are involved, and in our case there are 7, namely the flowrate Q, the power P, the head H, the rotational speed N, impeller diameter D, the fluid density ρ, and finally the fluid absolute viscosity, μ.

The functional relationship existing among these variables could be stated as follows:

$$F\ (Q,\ P,\ H,\ N,\ D,\ \rho\ ,\ \mu\ ) = 0 \tag{4.1}$$

Our three independent dimensions (m) are the mass M, length L and time t leaving us with four dimensionless parameters which could be stated as:

$$F\ (\Pi_1,\ \Pi_2,\ \Pi_3,\ \Pi_4) = 0 \tag{4.2}$$

The detailed derivation for these four coefficients can be found in texts by Stepanoff, Fox and McDonald or Shepherd [19,33,34], and therefore will not be included here. The resulting coefficients are:

$$\Pi_1(\text{capacity}) = \frac{Q}{D^3 N} \quad , \tag{4.3}$$

$$\Pi_2(\text{Head}) = \frac{(gH)}{N^2 D^2} \quad , \tag{4.4}$$

$$\Pi_3(\text{Power}) = \frac{P}{\rho\, D^5 N^3} \quad , \tag{4.5}$$

$$\Pi_4(\text{Reynolds}) = \frac{\mu}{\rho\, D^2 N} \quad . \tag{4.6}$$

These coefficients apply to our experimental analysis since our system can be regarded as dynamically similar with D and ρ being constant all the time. The affinity laws are developed from the above and can be stated for two different operating conditions as:

$$\frac{Q_1}{N_1} = \frac{Q_2}{N_2} \quad , \tag{4.7}$$

$$\frac{H_1}{N_1^2} = \frac{H_2}{N_2^2} \quad , \tag{4.8}$$

$$\frac{P_1}{N_1^3} = \frac{P_2}{N_2^3} \quad . \tag{4.9}$$

4.3 Flowrate Calculation

The flowrate of the pumped fluid was measured in the discharge side of the hydraulic loop. This was accomplished through the use of a stainless steel square edge orifice plate. In order to comply with the ASME fluidmeter standards for a 3-inch diameter pipe [35], two pressure taps were made 1.5 and 3.0 inches downstream and upstream of the plate, respectively. In order to minimize the eccentricity, the plate was press fitted into a flange and hence tightly secured with another flange.

The inlet diameter of the plate (orifice) was chosen to be 1.25 inches based upon the pump's rated flowrate of 181 gallons per minute for water. The flowrates were calculated with the aid of a standardized equation which transformed the plates differential pressure recordings into flowrate values. The flowrate Q is given in cubic feet per hour by:

$$Q = 359 \; K\beta^2 D^2 \left(h_w / \gamma\right)^{1/2} \quad , \tag{4.10}$$

where: K = a constant defined as $C\,(1-\beta^4)^{1/2}$

C = Coefficient of discharge

β = Ratio of orifice diameter to pipe inside diameter d/D, which is .407431.

D = Pipe inside diameter. For three inch PVC pipe of schedule 40 it is 3.068 inches.

d = Orifice diameter of 1.25 inches.

h_w = Differential pressure across the orifice plate in inches of water at 68° F.

γ = Specific weight of fluid. For water it is 62.4 lbs/ft^3 at 68° F.

The expression 359 $K\beta^2$ may be lumped into a single term called the principal meter constant, I. From the Flowmeter Computational Handbook [36] it is found to be 36.192. After performing the necessary unit conversions and rearrangement, equation 4.10 becomes

$$Q = (1000\ h_w \div 1.245)^{1/2}\ , \tag{4.11}$$

where the units are gpm and psi respectively for Q and h_w. During experimentation, the pressure differentials were measured by calibrated transducers which were connected to carrier demodulators and digital voltmeters. The readouts were converted into psi's according to the calibration of the transducers' diaphragm pressure rating. Experiments were performed at a range from fully open to shutoff. At the high speed condition the fully open flowrates approximately corresponded to 120 gpm's while it was around 90 gpm's at the low speed tests.

4.4 True Input Power and Rotational Speed

Since the panel wattmeters were designed to operate at normal frequencies (60 Hz), and we were to operate at 278 and 400 Hz, they needed to be calibrated. The two operating frequencies will be

referred to as the "high" and "low" speed throughout this study with 400 Hz being the high case. A special calibration circuit was set up by Prince [1], in which each panel wattmeter was preceded by a bench wattmeter. This detailed circuit diagram is included in Appendix A. Prince recorded both the panel and bench wattmeter readings during the initial part of his testing, and accounted for the bench wattmeter power loss due to the wattmeter current coil. He plotted the results for both the 1500 and 3000 wattmeters and they are reproduced here respectively as Figures 21 and 22. Resulting from the best fit straight lines he obtained the following correlation equations; for the 1500 wattmeter,

$$P_b = .92\ P_p - 21.52 \tag{4.12}$$

and for the 3000 wattmeter,

$$P_b = .85\ P_p + 127.46, \tag{4.13}$$

where all P units are to be in watts. Once a panel meter reading is taken the actual input power it represents is obtained from equations 4.12 and 4.13, irrespective of the operating speed.

The test pump is driven by the induction motor which goes through speed variations under different loadings. Since the speed variations were minimal the true rotational speed was obtained by using a first order correction based on the electrical input power (total of bench wattmeter readings). For the high speed case an input power versus rotational speed plot deduced from the motor manufacturer's data was used and it is reproduced as Figure 23. The best fit straight line equation obtained by Prince is:

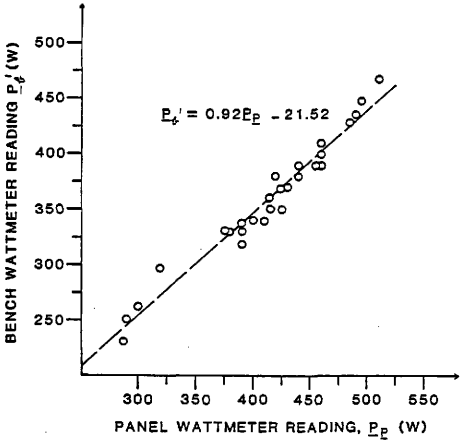

Figure 21. Calibration of the 1500 wattmeter.

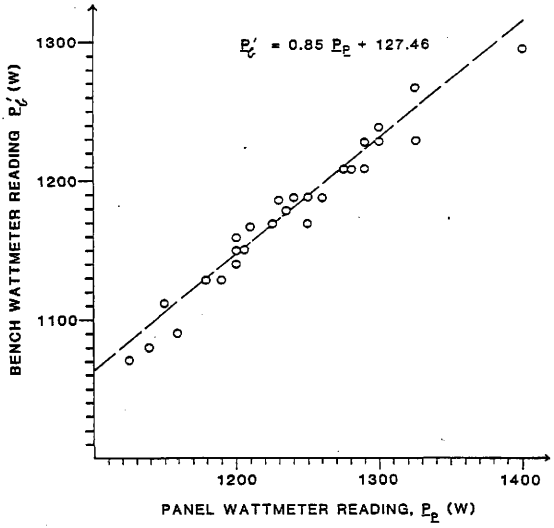

Figure 22. Calibration of the 3000 wattmeter.

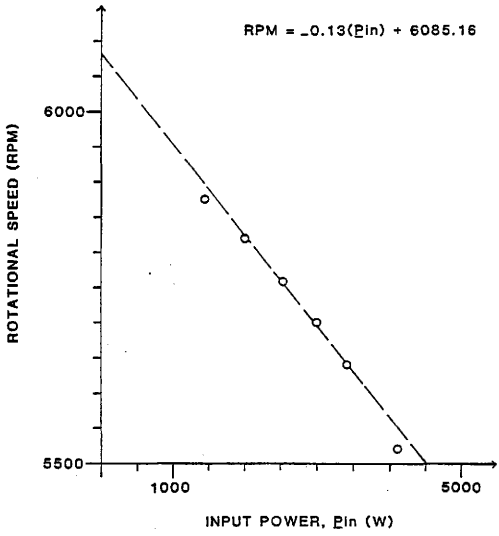

Figure 23. Pump Rotational speed vs. input power at high speed.

$$N = -0.13\ P_{in} + 6{,}085.16 \qquad (4.14)$$

where N is the rotational speed in shaft revolutions per minute (rpm) and P_{in} is the net input electrical power in watts. Since there were no low speed power data available, Prince ran two tests at shutoff conditions and developed Figure 24, where he represented the best fit line with:

$$N = -0.40\ P_{in} + 4{,}566.7 \qquad (4.15)$$

In the first test he ran the pump with water and in the second with air, but in both tests he measured the rotational speeds with a strobe light and accounted for frequency variations and copper losses. For the experimental operating range both speed equations should provide accurate values.

4.5 Test Procedure

The main purpose of this research is to study the effects of various inlet geometries on suction recirculation phenomena. Six different geometries were tested. The selection was made upon the basis that they would all be effective in delaying the onset of recirculation due to their certain design characteristics. Four epoxy cones were made with differing frustrum heights so that they would either partially or completely cover the inlet area of the axial impeller. At the pump inlet two piping configurations were tested, the first was a clear, straight plexiglass used at normal operating conditions and the other a U-shaped PVC assembly with its elbows

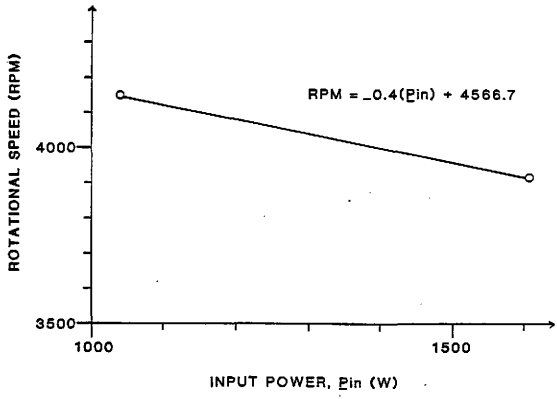

Figure 24. Pump rotational speed vs. input power at low speed.

serving to resist the recirculating flow. The other three geometries could be considered as inlet guide vanes or flow straighteners and were made in the shapes of a cone (nozzle), a cross (cruciform) and a box (channel). These inlet guide vanes were shown in Figure 17. All geometries were placed at the suction side of the pump since we were interested in recirculation occurring at the inlet. The flow guide vanes were all tested while they were installed in the plexiglass pipe and the conical vane was tested at three different upstream locations to determine the significance of vane distance away from the impeller plane. The conical covers were mounted on the inner pump casing and tested with both piping installations.

The flow velocities in the plexiglass pipe, both with and without the conical guide vane were measured by a five hole pitot probe. The electrical power input and voltages were recorded from calibrated panel meters. The suction pressures were recorded at three different inlet sections, with four pressure taps equally spaced circumferentially at each section. The experiment outline along with the crucial distances are presented in Table 1.

All experiments were carried out with the inlet valve always fully open, while the discharge valve was throttled to give an operating flow range from fully open to shutoff. In order to determine the effect of different operating speeds on recirculation, tests were performed at 5600 and 3800 rpm, respectively, the high and low speeds. The pressure and flowrate measurements were made with a system consisting of a differential pressure transducer, a carrier demodulator and a digital voltmeter, with the exception of the discharge pressures

Table 1. Experiment Outline and Important Locations

Inlet Geometry	High Speed	Low Speed	Velocity Meas.	Cones	Upstream loc. of geom. from impeller plane (inches)	Upstream loc. of suction pressure taps (inches)
Transparent straight pipe	X	X	X	X[1]	.963	.042, 1.338, 2.810
U-pipe	X	X		X	5.525[2]	.042, 1.373, 2.553
Conical Guide Vane	X	X	X		.382, 1.090, 1.817	.042, 1.338, 2.810
Cross Vane	X	X			.278	.042, 1.338, 2.810
Box Vane	X	X			.336	.042, 1.338, 2.810

[1] Performed by Prince [1].
[2] Up to elbow throat.

which were measured by a 60 psi pressure gauge. At each flowrate the upstream static pressure and the 12 suction pressures from the three sections were recorded with the aid of a switchboard system created from four 5-way ball valves described in the previous chapter (Fig. 18). The occurrence of recirculation was verified through a set of strings placed in the plexiglass pump inlet, since they reversed their directions with the successive reductions of the flowrate.

The results obtained from these tests will be presented and correlated with each other, and compared to previous studies and checked with a proposed analytical theory.

4.6 Input Shaft Power

The variation of the shaft input power with different inlet geometries constituted an important part of this study. Even though our main concern was the determination of the critical flowrates, the pump shaft power consumption characteristics were given special attention in order to select the overall ideal inlet geometry parameter. The detailed procedure of determining the input shaft powers was described by Prince [1]. For completeness, it is given in Appendix B.

All input shaft power values determined from experimental data and calculations were plotted with respect to flowrates and are presented in Figures 25 to 34. The graphs are arranged in the chronological order of the tests starting with the straight plexiglass pipe, followed with the U-pipe with and without the four conical impeller covers, the conical inlet guide vane at three different upstream locations, and finally the cross and box type vanes. For each geometry the low and high speed results are presented successively.

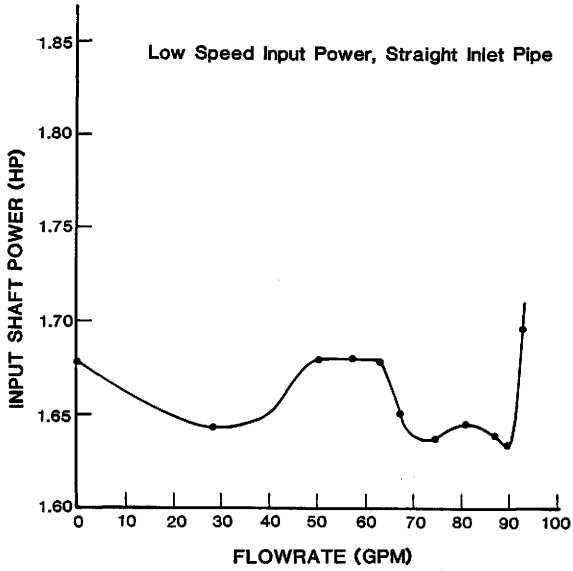

Figure 25. Low speed shaft power variation with flowrate for straight pipe.

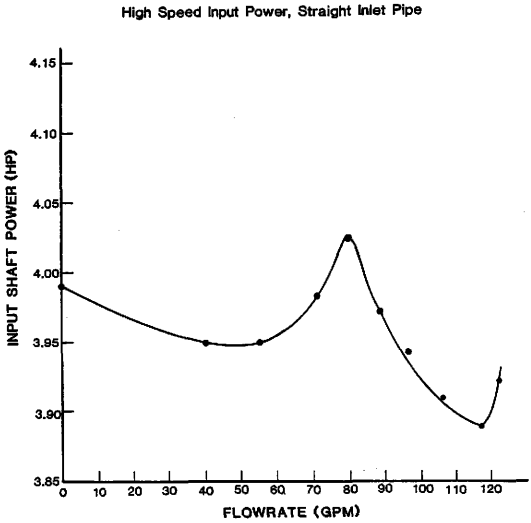

Figure 26. High speed shaft power variation with flowrate for straight pipe.

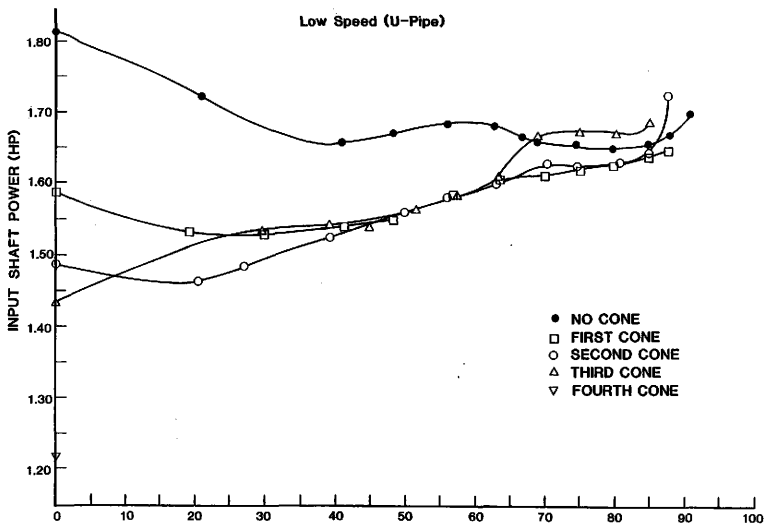

Figure 27. Low speed shaft power variation with flowrate for U-pipe and conical covers.

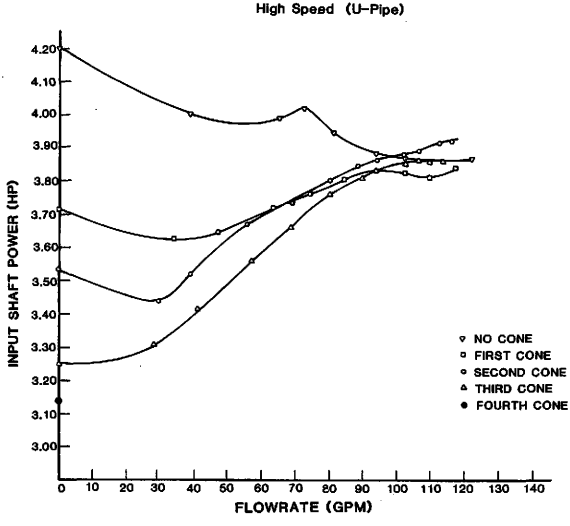

Figure 28. High speed shaft power variation with flowrate for U-pipe and conical covers.

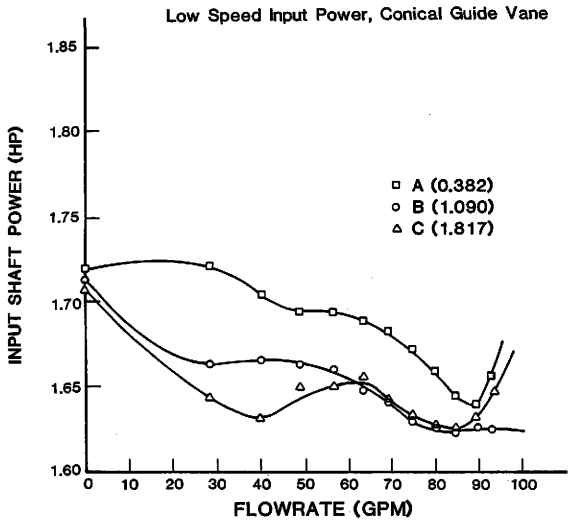

Figure 29. Low speed shaft power variation with flowrate for the conical inlet guide vane.

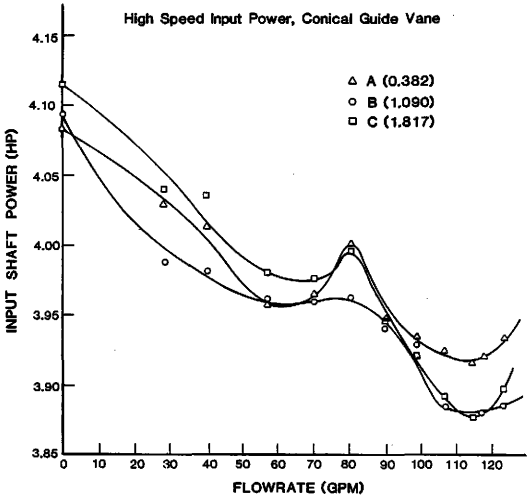

Figure 30. High speed shaft power variation with flowrate for the conical inlet guide vane.

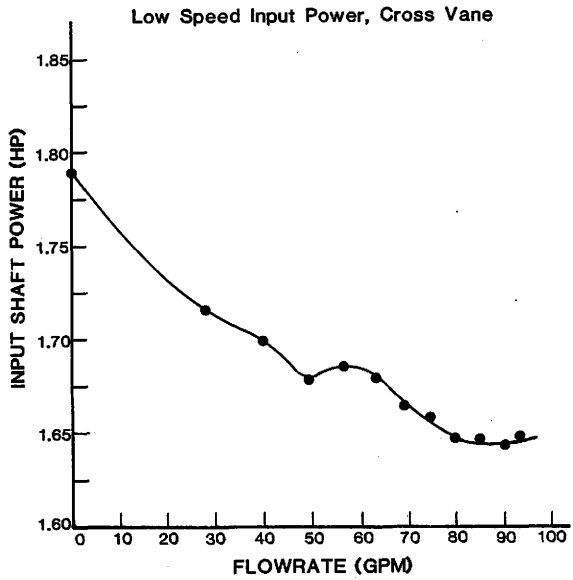

Figure 31. Low speed shaft power variation with flowrate for cross vane.

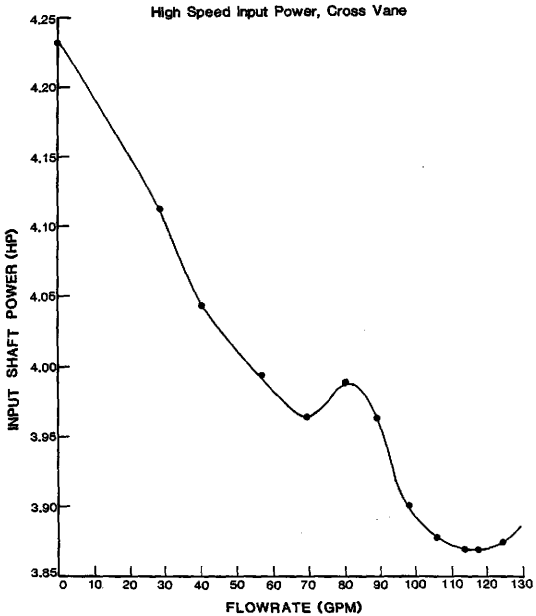

Figure 32. High speed shaft power variation with flowrate for cross vane.

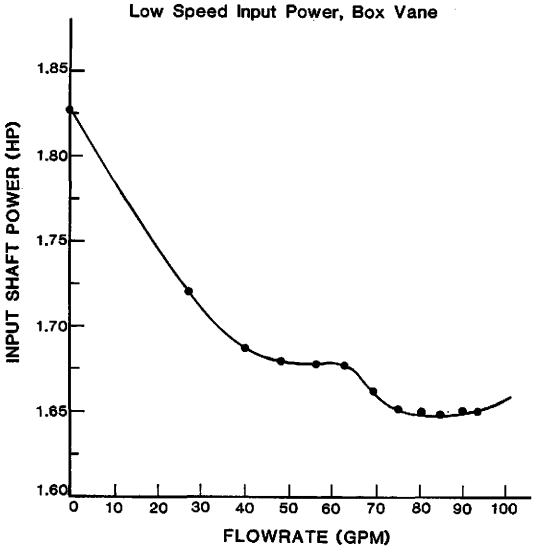

Figure 33. Low speed shaft power variation with flowrate for box vane.

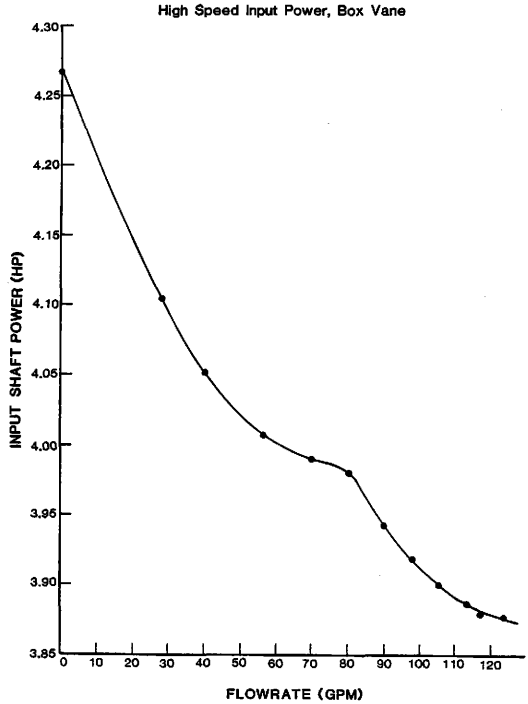

Figure 34. High speed shaft power variation with flowrate for box vane.

A large number of results could be drawn from the above figures but only the more significant and relevant ones are to be discussed here. The first test was performed with the clear plexiglass pipe and could be regarded as a repetition of the Prince experiment for the no cone case (Figs. 25 & 26). Both numerically and formwise the results compare quite well with Prince's experiment indicating consistency of experimental procedure. The second set of tests were carried out in a manner very similar to Prince's, but in our case the straight plexiglass pipe was replaced with the U-pipe assembly (Figs. 27 and 28). Our goal was to determine the effects of different inlet piping and area reductions on the pump power consumption and recirculation. The inlet area reduction was achieved with the aid of four cone covers where the last one was designed to cover the whole impeller inlet area. With the fourth cone installed, no flow was recorded and its power reading served only as a reference point.

At high flowrates all data points seem to be clustered together, but as the flow is decreased the curves tend to separate and at very low flows they are clearly distinguished from each other. A very important observation is that, as the pump inlet area is decreased the shaft power consumption decreases, and this fact is further accelerated with the decreasing flowrates. It is worthwhile to note that for the no cone, first and second cone cases we have negative shutoff slopes, while this trend is reversed to positive with the third cone. This shift might be linked with the severe inlet area reduction. A detailed comparison of the results of these two experiments with Prince [1] will be done in the fifth section of Chapter 5.

The conical guide vane was tested at three different pump upstream locations and the results are presented in Figures 29 and 30. The different distances seem to have no visible effect on pump power consumption at high speeds, however this observation does not appear to be true for low operating speeds. From Figure 29 it is obvious that when the vane is located closer to the impeller plane, the pump draws more power, while the characteristics at the other two locations still do not differ significantly. At high speeds the power curves for all three cases frequently intersect each other, even to the point where the shutoff power values are completely reversed in order, with respect to the low speed recordings. Although the power values at shutoff are reversed in order with the change of speed, it is important to note the closeness of the magnitudes of these values. The speed factor has only been crucial for this test, while all the other low and high speed tests, the results are consistent with each other. Quantitatively speaking, as the speed is increased, the power consumption is also increased as this can be seen from all collected data.

Last set of tests were carried out with the cross and box type flow guide vanes (straighteners), Figures 31 to 34. The most remarkable feature common to both of these as well as to the conical vane is the fact that as flowrates are decreased the pump power consumption is increased. It also might be interesting to note that the power values of the cross vane are slightly higher than the box vanes. Since the cross vane was installed closer to the pump, the result supports our findings with the conical vane.

Since the shutoff power consumption values were available from all tests and that it is a commonly referred point by all pump users, it was preferred to compare results at shutoff. Even though this comparison may not hold for the whole flow range, it could be regarded as a good indication of the pump power consumption characteristics. All shutoff power readings obtained are presented in a comparative manner in Table 2. From the table it can immediately be seen that the box and cross vanes would be undesirable, while the conical vane values are very close to each other and are comparable with the straight pipe values. The U-pipe results with the cones seem to be ideal, proving the inlet area reduction as the most effective power consumption parameter. From the no cone to the third cone case a 22.6 and 20.8 percentage reduction of power consumption is obtained for the high and low speeds respectively. The values in Table 2 will be used in Chapter 5 to correlate power and flowrate in a nondimensional manner.

Hydraulic power is regarded as the main component of the total pump power consumption. However, power drawn by recirculation and mechanical losses also constitute a main portion of this consumption. The input shaft power behavior seen in Figures 25 to 34 can be attributed to the recirculatory power. Behaving like a third order polynomial this component causes the peaks and dips in the power distribution. This point will be further discussed in Section 5.6.

4.7 Pump Head and Overall Efficiency

By measuring the differential pressure across the pump, and by monitoring the input power and flowrate values, Prince [1] was able to

Table 2. Shutoff Shaft Power Consumption for Inlet Geometries

Rotational Speed (RPM)	SHUTOFF SHAFT POWER CONSUMPTION (HP)										
	Straight Plexi Pipe	U-PIPE					Conical Vane			Cross Vane	Box Vane
		-	1	2	3	4	A	B	C		
High (5600)	3.990	4.200	3.718	3.535	3.250	3.140	4.085	4.095	4.115	4.235	4.270
Low (3800)	1.680	1.810	1.585	1.486	1.433	1.216	1.720	1.712	1.709	1.792	1.828

- = No cone
1 = Cone #1
2 = Cone #2
3 = Cone #3
4 = Cone #4

A = First location of con. vane (.382")
B = Second location of con. vane (1.090")
C = Third location of con. vane (1.817")

obtain the pump performance curves. Since the pump and test rig used by Prince was also used in this study with a few minor changes, it was decided that there was no need to repeat his findings and so his results for total head and overall efficiency for both speeds are reproduced in Figures 35 to 38. Prince took 3800 and 5600 as base rpm values and used the affinity laws (equations 4.7 and 4.8) to correct for all varying head and speed readings. A sample calculation procedure to determine the pump's power, head and efficiency characteristics at both speeds can be found in his Appendix C.

The overall efficiency, η_o, was calculated based on the gross power input to the pump, and the power obtained from the pumped liquid in the form of

$$\eta_o = C\ (H \times Q) \div P_{in} \qquad (4.16)$$

where C is a conversion coefficient.

The main conclusions of Prince could be summarized as: at the recirculation free high flowrates, the decrease of the inlet area decreases the head produced while at low flowrates below the critical zone, it causes an increase in the head produced. The effect of swirl on head at low flows should be accounted for to obtain correct readings. As it might be expected from previous conclusions, at low flowrates the efficiency slightly increases. The rated flowrate by the manufacturer is never reached as it can be seen from the efficiency curves, and this might be due to the elbow and straightener located at the pump discharge acting as flow resistors, and to the radial stage

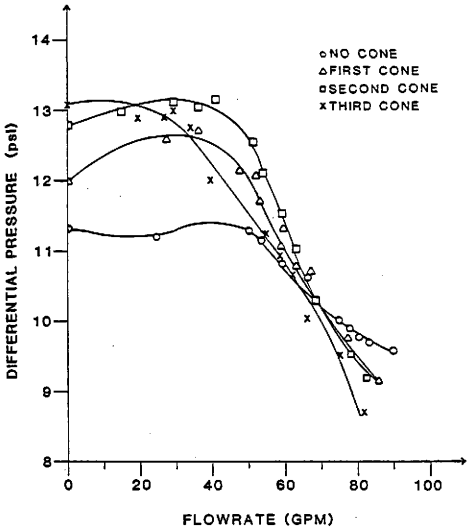

Figure 35. Low speed pump head performance for the straight pipe and conical covers.

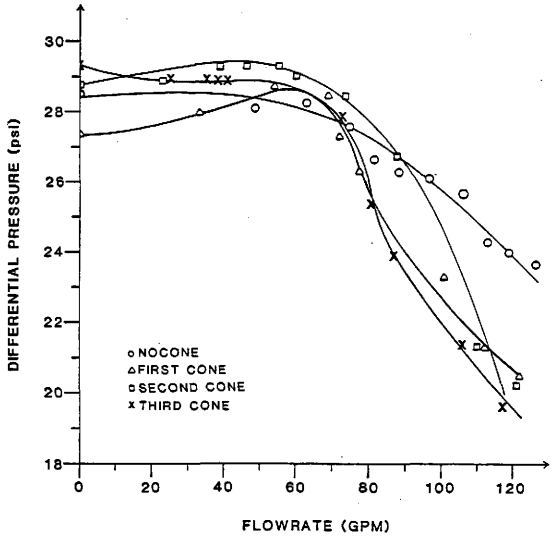

Figure 36. High speed pump head performance for the straight pipe and conical covers.

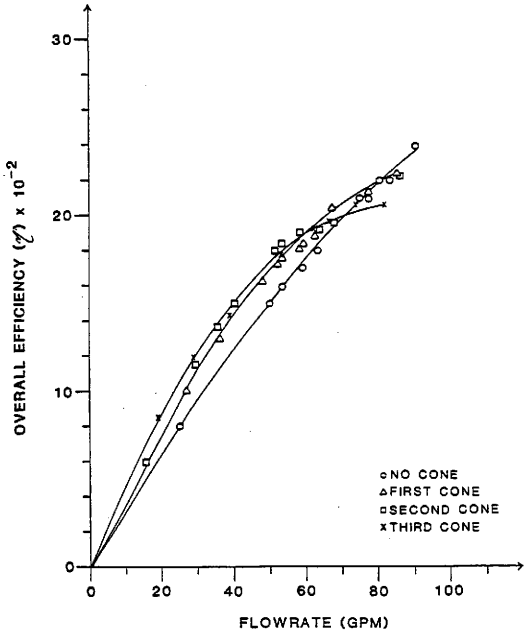

Figure 37. Low speed pump overall efficiency for straight pipe and conical covers.

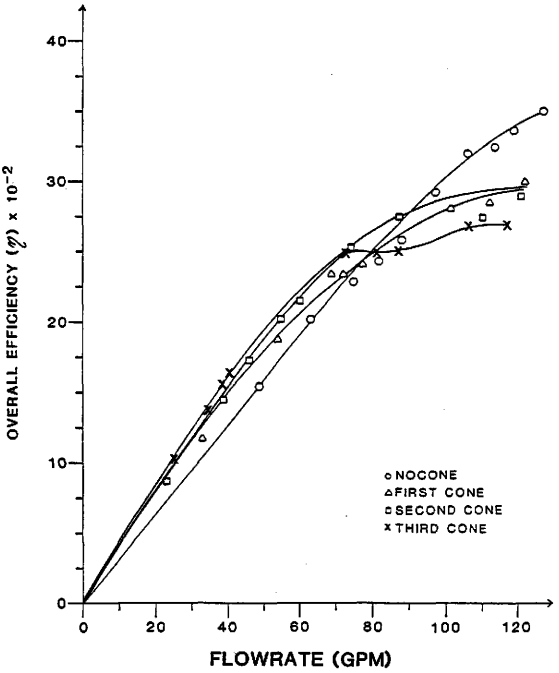

Figure 38. High speed pump overall efficiency for straight pipe and conical covers.

which remained nonoperational throughout this study. However, this is not a serious problem, because we are mainly interested in suction recirculation which only occurs in the relatively low flowrates. All results are valid for both of the operating speeds.

It can safely be concluded that the head and efficiency results presented here are viable for all tests performed in this study. However, contradictory to the conical covers, the conical inlet guide vane produced comparable differential pressures with the straight pipe also at the recirculation free high flowrates, this can be seen in Figure 39.

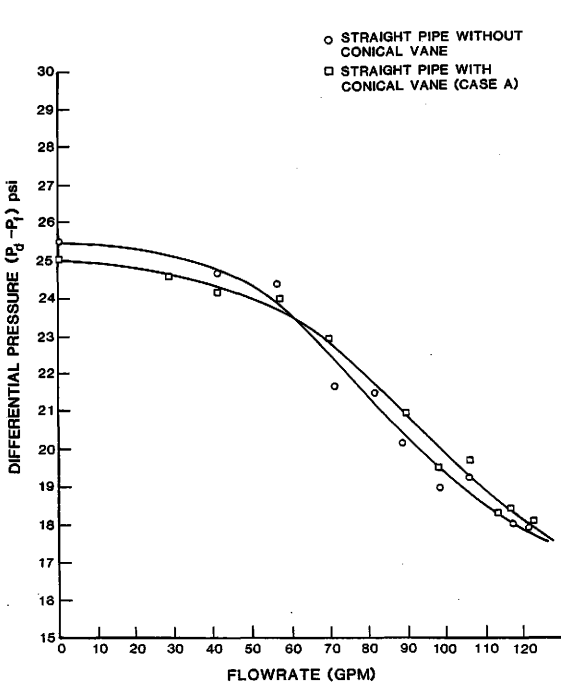

Figure 39. High speed pump head performance for straight pipe with and without the conical inlet guide vane.

CHAPTER V. EXPERIMENTAL RESULTS AND DISCUSSION

5.1 Critical Flowrate Determination

Flow recirculation has been studied by numerous investigators, but only a few of them have actually determined the critical flowrate, Q_{cr} at which the reverse flow is initiated. Visual observation of string motions, velocity and pressure measurement techniques have been proven to be the most effective ways to determine this crucial point. The studies done by Prince [1] and the author were planned to complement each other and since Prince utilized the "string" method to find the critical flowrates, the "pressure detecting" method was adopted for this study.

In the "string" method, a set of nylon strings are installed in the clear plexiglass pipe so that they would extend into the flow region. As the flowrate is gradually decreased the strings start to reverse from their normal flow direction, and the point where the reversal occurs is called the "critical flowrate." In the "string" method the strings were placed circumferentially at three different upstream test sections, the section closest to the pump being designated as the "first section." When the flow reversal was observed at this section it was referred to as the "first section critical flowrate," Q_{r1}, and the last (most upstream) one being the "third section critical flowrate," Q_{r3}. This nomenclature will be used throughout this study.

In the pressure technique three different test sections are designated again, but in this case the strings are replaced by pressure taps. Each test section has four pressure taps distributed circumferentially at 90 degrees apart. A special pressure control board was prepared where we could easily connect to a desired pressure tap at any section and record its pressure with a differential pressure transducer. The four circumferential pressure readings taken at each section were averaged and were deducted from the upstream static pressure, which served as a reference point since it was never affected by recirculation. The differential pressure values ($P_{av}-P_f$) for each of the three test sections were plotted against the flowrate, which ranged from fully open to shutoff. All test results clearly indicated the presence of two pressure trends. Initially, at high flowrates we observe low pressures, but at a certain point the pressure suddenly increases and this increase steadily continues with the gradual decrease of the flowrate. The high and low pressure zone data points were each fitted with best fit straight lines and the discontinuity point where they intersected was designated as the "section critical flowrate." In each graph three of these flowrates were obtained, with the section closest to the pump having the highest value. The case when the conical inlet guide vane was located 1.09 inches away from the impeller plane is provided as a sample for the abovementioned procedure in Figures 40 and 41 for the low and high speeds respectively. The flowrate values are given in orifice pressure units.

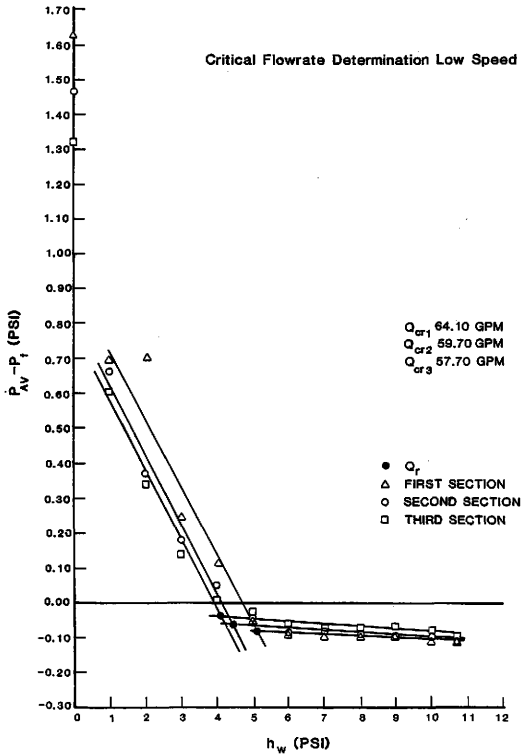

Figure 40. Low speed section critical flowrate determination for case B of the conical guide vane.

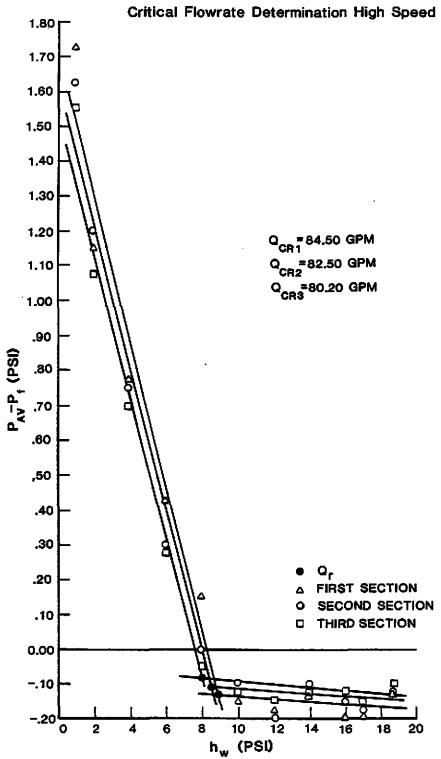

Figure 41. High speed section critical flowrate determination for case B of the conical guide vane.

The three section critical flowrates are then plotted with respect to the corresponding distances from the pump's inlet plane. These distances for all cases were presented in Table 1, and are normalized with the suction pipe's inlet diameter. In all plots the procedure of Sen [17] is followed, a straight line is fitted to the three section critical flowrate points and the point where this line intersects the vertical axis is taken as the "pump critical flowrate," Q_{cr}. This is viable since the vertical axis represents the pump inlet plane location. The graphs presenting all critical flowrates obtained for the straight pipe, U-pipe, and conical guide vane tests are shown in Figures 42 to 46 for both speeds. It is important to note the deviation of the upstream data points from the best fit line of Figure 44. This is probably due to the secondary flows, created at high speeds by the U-pipe's elbow, affecting the two upstream test sections. For clarity and comparative purposes, the pump and sectional critical flowrates determined from all tests are summarized in Table 3. Since the geometry of the box and cross vanes interfered with the second and third section pressure taps, the faulty readings were discarded.

All the best fit lines depicted in Figures 42 to 46 have negative slopes, indicating that the section critical flowrates are a decreasing function of the upstream distance. This relation could be explained with the fact that the strength of the swirling recirculatory flow increases with a decrease in the through flowrate. The different slopes of the best fit lines do not permit any definite conclusions with regard to the rate of decay of the swirling reverse flow.

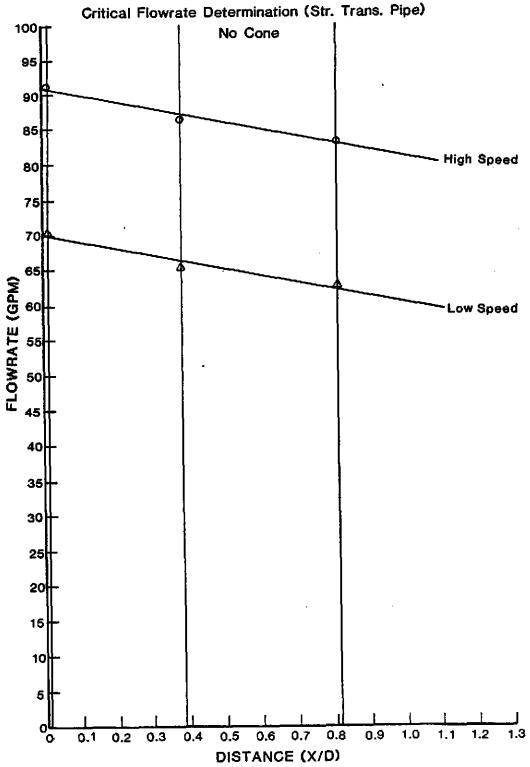

Figure 42. Pump critical flowrate determination for the straight pipe, at both speeds.

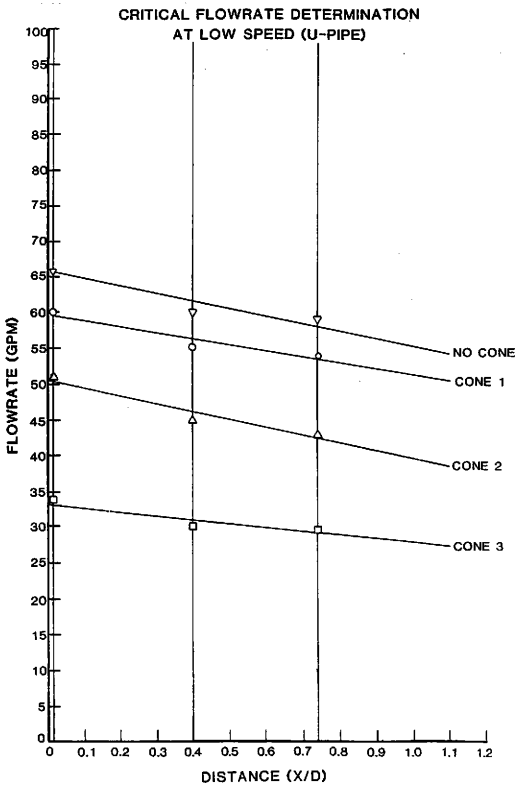

Figure 43. Low speed pump critical flowrate determination for the U-pipe.

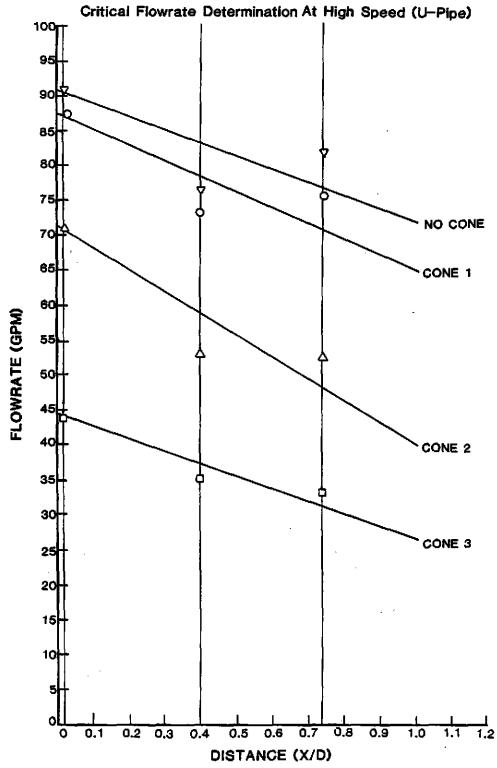

Figure 44. High speed pump critical flowrate determination for the U-pipe.

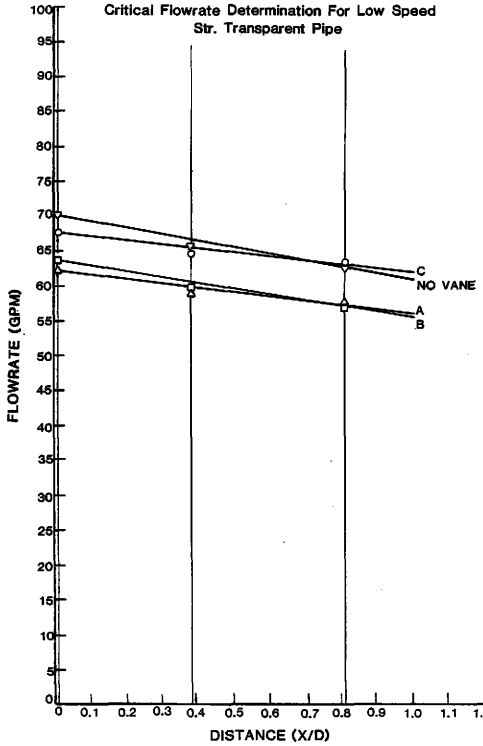

Figure 45. Low speed pump critical flowrate determination for the conical guide vane.

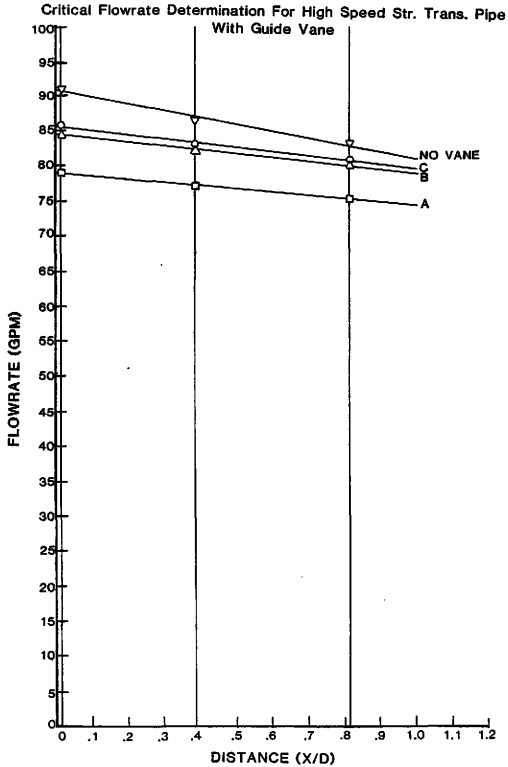

Figure 46. High speed pump critical flowrate determination for the conical guide vane.

Table 3. Section and Pump Critical Flowrates (GPM)

Q_{cr}	Transp. Pipe		U-Pipe								Conical Guide Vane						Cross Vane		Box Vane	
	Low	High	Low				High				Low			High			Low	High	Low	High
			–	1	2	3	–	1	2	3	A	B	C	A	B	C				
Q_p	70.5	91.3	66.7	60.4	51.1	33.8	91.7	88.7	72.6	44.3	62.5	64.2	68.2	79.3	84.6	86.1	–	–	–	–
Q_{r1}	70.3	91.2	66.5	60.1	50.7	33.5	90.5	87.4	71.1	43.9	62.4	64.1	68.0	79.2	84.5	86.0	64.3	85.0	67.8	90.7
Q_{r2}	65.6	86.7	60.1	55.3	44.8	30.4	81.4	75.3	52.6	34.7	59.1	59.7	64.8	77.4	82.5	83.1	–	–	–	–
Q_{r3}	62.7	83.4	58.8	54.2	43.0	29.7	76.1	73.1	52.3	32.9	57.4	57.7	63.4	75.4	80.2	81.2	–	–	–	–

Abbreviations

Q_{cr} = Critical flowrates
Q_p = Pump crit. flowrate
Q_{r1} = First test section crit. flowrate
Q_{r2} = Second test section crit. flowrate
Q_{r3} = Third test section crit. flowrate

– = No cone
1 = Cone #1
2 = Cone #2
3 = Cone #3

A = First location of con. vane (.382")
B = Second location of con. vane (1.090")
C = Third location of con. vane (1.817")

Since the best efficiency flowrate was never attained, it was not possible to normalize the critical flowrates with respect to it, as it was hoped for. The slight variation of the impeller rotating speed with respect to the input power was also taken care of with the extrapolation technique mentioned above.

A careful analysis of Table 3 supplies us with the following results. In delaying the inception of suction recirculation, a) the U-pipe on the average is 6% more effective than the straight pipe, b) placing guide vanes in the inlet of the straight pipe provides an improvement of 8% and 3% on the average respectively with the cases when the straight and U-pipes are tested by themselves, c) the most effective inlet guide vane is the conical design, which enhances higher flow velocities at the outer radius of the pump inlet, d) by bringing the conical inlet guide vane 1.5 inches closer to the pump inlet plane the vane effectiveness has increased on the average by 8%, and most importantly, e) reducing the inlet area seems to be the most effective delaying technique. The third cone is on the average 50% more effective than the no cone case of the U-pipe.

It is interesting to note that for both speeds, the critical flowrates were initiated at a range of 50 to 60% of the design flowrate, and when the third cone was installed this rate was reduced to 25%. Comparisons of the "pressure" and "string" techniques, as well as their numerical results will be discussed in Section 5 of this chapter.

5.2 Recirculation Power Correlation

The pump power consumption associated with the suction recirculation will be correlated with the fluid flowrate and the Reynolds number. The idea of correlating important pump parameters is based on a study performed by Mann and Marston on rotating disks [37]. The nondimensional parameters they used were the "Moment Coefficient, C_m" and the "disc Reynolds number, Re," defined as

$$C_m = \frac{T}{\rho\omega^2 R^5} \quad , \quad Re = \frac{\omega R^2}{\gamma} \tag{5.1}$$

where T is the torque applied to the disc, ω the angular velocity and R the disc radius. The moment coefficient can easily be converted to the power coefficient by multiplying both its numerator and denominator by ω. The power coefficient to be correlated with the Reynolds number is obtained as:

$$\Pi_3 = \frac{P}{\rho N^3 D^5} \tag{5.2}$$

where P is the power loss due to suction recirculation, N the corresponding rotational speed at shutoff, and D the characteristic dimension.

Since tests performed with conical covers proved to be the most effective flow recirculation delaying technique and covered a wide range of shutoff power readings, results for these tests were correlated. With the conical covers, partial reductions of the impeller inlet area is achieved and this in effect will reduce the recirculating flow and its associated power consumption. Covering the inlet

area completely should almost eliminate the total recirculation power consumption even at the shutoff condition, except for an insignificant amount of power associated with the short-circuit recirculating flow within the impeller. The geometry and the characteristic dimensions of the four cones used for this study are shown in Figure 47. The fourth cone completely covers the inlet area. The test section geometry with a partial cone installed on the pump inner housing was given in Figure 16.

In his study, Prince [1] has tried three characteristic inlet dimensions in correlating his data, the first being the geometric radius, r_t, from the impeller axis to the cone tip, the second r_s, based on the open inlet area of the frustrum of the cone, and finally r_h, the hydraulic radius accounting for the impeller inlet area and shape. Upon completion of his analysis, Prince concluded that the most significant inlet parameter was the hydraulic radius. Therefore, in our correlation, only the hydraulic radius was used, it is defined as:

$$r_h = 2A \div S \tag{5.3}$$

where A is the open area and expressed as

$$A = \frac{\pi}{\sin\alpha} \quad (r_t^2 - .55^2) \tag{5.4}$$

with α being the angle of inclination for the cone. The wetted perimeter, S, is taken as the sum of the circumferences of the two circles having .55 inches and r_t as their respective radii, i.e.,

$$S = 2\pi \ (.55 + r_t) \ . \tag{5.5}$$

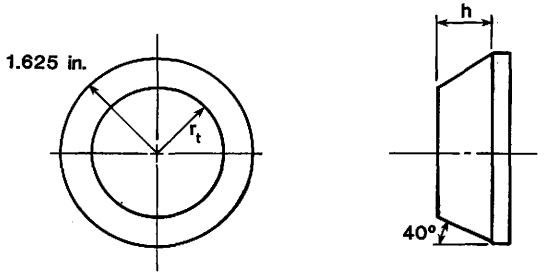

CONE	h (in.)	r_t (in.)	r_h (in.)
1	0.475	1.23	1.05
2	0.700	1.04	0.76
3	0.818	0.94	0.60
4	1.281	0.55	0.00

(c)

Figure 47. Characteristic dimensions of the conical covers.

After substituting equations (5.4) and (5.5) into (5.3), we finally obtain:

$$r_h = 1.556\ (r_t - 0.55) \tag{5.6}$$

The respective r_t and r_h values in inches were presented in Figure 47 for all cones.

Since the fourth cone completely covers the impeller inlet for no through flow, the power measurement with this cone excludes suction recirculation power, while measurements with other cones include certain amount of power due to suction recirculation. Hence the power consumptions associated with the recirculating flow at shutoff conditions can be obtained by subtracting the power requirements of the fourth cone from any of the other cones. The resulting recirculation powers represented by P was used in equation (5.2) to determine the nondimensional power coefficient, Π_3. However, this equation needs to be modified to take care of unit conversions and constants. For a water density of 62.32 lbm/ft^3 at 68° F, equation (5.2) takes its final form as:

$$\Pi_3 = 1.9243 \times 10^9 \frac{P_r}{N^3 r^5} \tag{5.7}$$

where P is in horsepower, r is in inches and N is in rpm. In a similar manner and for a kinematic viscosity of 1.074×10^{-5} ft^2/s, the Reynolds number becomes:

$$Re = 67.7\ N\ r^2 \tag{5.8}$$

where again N is in rpm and r is in inches. The experimental values of P and N as well as calculated values of β and Re are given in Table 4 for the respective hydraulic radii at both speeds for both suction piping installations. The correlations obtained from data in Table 4 is plotted on log-log scale and is presented in Figure 48. This figure certifies the fact that reducing the impeller inlet area is a very effective means to reduce the suction recirculation power loss. The exponential increase of power savings with decreasing hydraulic radius is also verified.

Power consumption due to the suction recirculation at finite through flow can also be determined from the shaft power measurements with and without inlet partial coverings. At a certain flowrate, when the inlet partial cover just eliminates the recirculating flow, which will otherwise exist without the cover, the difference in shaft power measurements with and without the cover can be ascertained to be due to the suction recirculation of the open impeller. The test data is correlated by the power and flow coefficients. The flow coefficient, ϕ, is defined as the ratio of the measured flowrate over the best efficiency flowrate. The hydraulic radius is used again as the characteristic length to determine the power coefficient. The power lost due to recirculation and its corresponding flowrate, along with the dimensionless coefficients are given in Table 5. The power coefficient, Π, and the flow coefficient in the form of $(1-\phi)$ are plotted on log-log scale, the resulting graphs for both speeds are presented in Figure 49. The best efficiency point was never reached experimentally, but it was determined to be around 180 gpm at high speeds, from

Table 4. Shutoff Power Coefficient and Reynolds number data based on the hydraulic radius

			Straight Plexiglass Pipe				U-Shaped Pipe			
Freq (Hz)	Cone	Hydraulic Radius (inches)	P_r (HP)	N (RPM)	Re (10^6)	Π_3 (10^{-2})	P_r (HP)	N (RPM)	Re (10^6)	Π_3 (10^{-2})
278	-	1.48	.400	3918	.5810	.1802	.594	3819	.5663	.2890
278	1	1.05	.280	3984	.2974	.6726	.369	3955	.2952	.8993
278	2	.76	.200	4029	.1575	2.3820	.270	4008	.1567	3.1830
278	3	.60	.070	4068	.0992	2.6010	.217	4035	.0983	8.1740
400	-	1.48	1.090	5545	.8223	.1733	1.06	5495	.8149	.1731
400	1	1.05	.620	5626	.4199	.5220	.578	5603	.4182	.4954
400	2	.76	.370	5668	.2216	1.5540	.395	5634	.2203	1.6760
400	3	.60	.260	5688	.1386	3.3570	.110	5679	.1384	1.4860

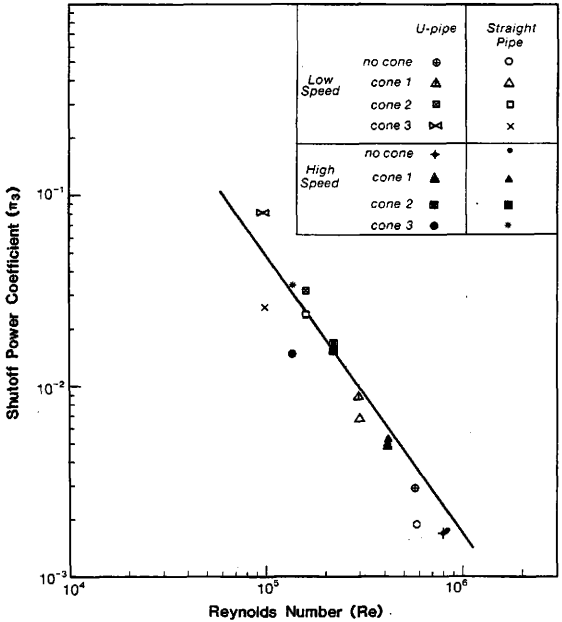

Figure 48. Correlation of shutoff power coefficient (Π_3) with Reynolds number (Re)

Table 5. Power and flow coefficients for the recirculatory flow range

	Straight Plexiglass Pipe					U-Shaped Pipe				
Freq (Hz)	Q (GPM)	P_r (Hp)	Π	$\phi = \frac{Q}{Q_o}$	$1 - \phi$	Q (GPM)	P_r (Hp)	Π	$\phi = \frac{Q}{Q_o}$	$1 - \phi$
278	0	.400	1.80×10^{-3}	0	1	0	.594	2.89×10^{-3}	0	1
278	38	.095	4.64×10^{-4}	.311	.689	38	.135	6.60×10^{-4}	.311	.689
278	57	.050	2.44×10^{-4}	.467	.533	54	.110	5.38×10^{-4}	.443	.557
278	65.5	.045	2.20×10^{-4}	.537	.463	62.5	.075	3.67×10^{-4}	.512	.488
400	0	1.090	1.73×10^{-3}	0	1	0	1.060	1.73×10^{-3}	0	1
400	52	.430	6.67×10^{-4}	.289	.711	50	.485	7.53×10^{-4}	.278	.722
400	77	.180	2.79×10^{-4}	.428	.572	78	.190	2.95×10^{-4}	.433	.566
400	88	.150	2.33×10^{-4}	.489	.511	90	.070	1.08×10^{-4}	.500	.500

Note: Power coefficient based on hydraulic radius and Q_o (high) = 180 gpm, Q_o (low) = 122 gpm.

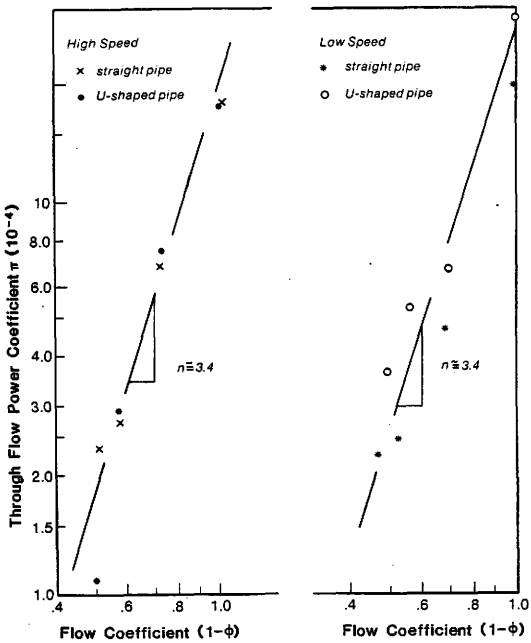

Figure 49. Correlation of through flow power coefficient (Π) with flow coefficient (1-ϕ).

the manufacturer's data. All the test data seems to correlate very well along a straight line when plotted on log-log scale. From Figure 49, it can therefore be deduced that the power consumption associated with suction recirculation is more dependent on the impeller inlet geometry rather than the suction pipe configuration. It is important to note that the shutoff values of Figure 49 are slightly off from the best fit line, and this deviation was emphasized when drawing the straight line of Figure 48. The data of Figure 49 can be correlated with:

$$\Pi = \Pi_3 (1-\phi)^n . \tag{5.9}$$

In dimensional form, it becomes

$$P_r = \Pi_3 \rho \omega^3 D_h^5 \left(1 - \frac{Q}{Q_o} \right)^n \tag{5.10}$$

or,

$$P_r = \Pi_3 \rho \omega^3 \left[\frac{2A}{\pi(r_2 + r_1)} \right]^5 \left(1 - \frac{Q}{Q_o} \right)^n \tag{5.11}$$

where r_1 and r_2 are the hub and tip radii of the impeller leading edge, and "n" is the slope of the best-fit straight lines of Figure 49. This correlation is very similar to the one suggested by Tuzon [32]. It will be further discussed in the last section of this chapter.

5.3 Critical Flowrate and Geometry Correlation

Since critical flowrate is the main parameter of our study, it is essential that we determine its behavior with respect to the pump inlet geometry. Correlating these two important parameters will not

only serve to determine the effect of inlet geometries on critical flowrates, but the result will also serve as a reference for pump users and future studies. As mentioned in Chapter 4, the main parameters involved with flow recirculation are Q, N, ρ, μ, r_i and r_h, where r_i is the impeller radius. A dimensional analysis similar to the one developed in Chapter 4 with N, ρ and r_h being the repeating variables was performed. The three resulting dimensionless parameters are as follows:

$$D_1 = \frac{Q}{Nr_h^3} = \Pi_1 \quad , \tag{5.12}$$

$$D_2 = \frac{\mu}{\rho N r_h^2} = \frac{1}{Re} \quad , \tag{5.13}$$

$$D_3 = \frac{r_i}{r_h} \quad . \tag{5.14}$$

D_1 is the capacity coefficient obtained in equation (4.3), while D_2 could be regarded as a form of the inverse of the Reynolds number, where r_h and $r_h N$ are the characteristic length and velocity, respectively. After substituting the constants and performing the unit conversions, equations (5.12) and (5.13) take the forms of:

$$\Pi_1 = 4.59 \frac{Q_{cr}}{Nr_h^3} \quad , \tag{5.15}$$

$$Re = 67.7\ Nr_h^2 \quad , \tag{5.16}$$

where Q, N, and r_h are in gpm, rpm and inches respectively. The Q used in equation (5.15) is the pump critical flowrate corresponding to

the flowrate at which the reverse flow is initiated at the impeller tips. The N used in both the above equations is the pump rotational speed corresponding to the Q, and finally r_h is the hydraulic radius, the most significant inlet geometry parameter.

In his study, Prince [1] plotted the capacity coefficient with respect to both the Reynolds number and D_3. From his analysis, he concludes that the primary parameter effecting the critical flowrate is the impeller inlet geometry, while the Reynolds number effects are secondary. He continues to stress that the Reynolds number is less significant in predicting the critical flowrate, but it should not be entirely neglected since recirculation also depends on viscosity. However, in our study we will only emphasize on the more significant inlet parameter, namely D_3.

Since the inlet guide vanes do not alter the inlet geometry of the pump (i.e., constant r_h), they cannot be used for this analysis. Therefore, the straight and U-shaped inlet pipings with and without the conical impeller covers will be analyzed and the results presented here. The D_3 and Π_1 values together with the other relevant parameters are presented in Table 6, while the impeller has a constant radius of 1.5 inches. The correlation of Π_1 and D_3 on log-log scale is given in Figure 50 for both piping installations. The trend can be verified as the r_1/r_h ratio increases with the decrease of the inlet cone areas. The data obtained for each cone case, irrespective of the inlet piping, indicates the consistency and accuracy of the experimentation technique. The results for cone number 3 seem to slightly deviate from the straight line trend, this is expected, since D_3 will

Table 6. Capacity Coefficient and Inlet Geometry Parameter

				Straight Plexiglass Pipe			U-Shaped Pipe		
Freq (Hz)	Cone	r_h (inches)	r_i/r_h	Q_{cr} (gpm)	N_{cr} (rpm)	Π_1	Q_{cr} (gpm)	N_{cr} (rpm)	Π_1
278	-	1.48	1.01	70.20	3915	.025	66.70	3910	.024
278	1	1.05	1.43	65.60	3923	.066	60.40	3951	.060
278	2	.76	1.97	57.50	3933	.153	51.05	3970	.135
278	3	.60	2.50	36.10	4009	.191	33.75	3982	.176
400	-	1.48	1.01	107.10	5586	.027	91.65	5570	.023
400	1	1.05	1.43	88.80	5602	.063	88.65	5586	.062
400	2	.76	1.97	76.60	5607	.143	72.55	5598	.136
400	3	.60	2.50	49.80	5664	.187	44.25	5650	.163

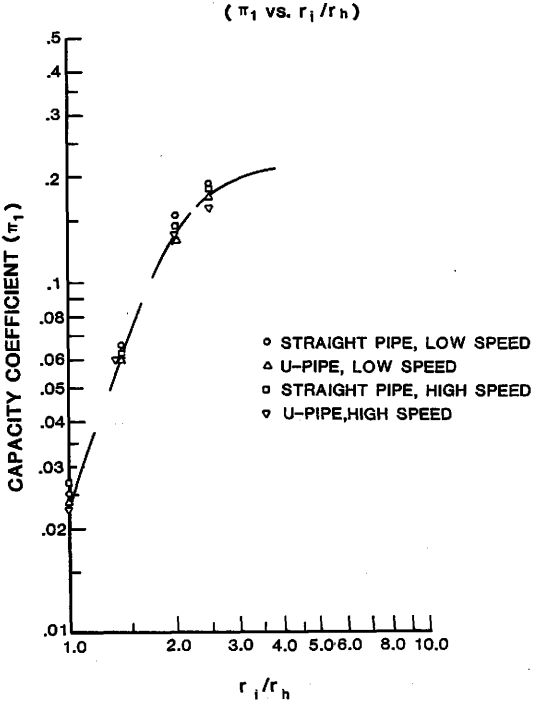

Figure 50. Correlation of capacity coefficient (Π_1) with inlet geometry parameter (D_3).

approach infinity as r_h is decreased. The correlation of data indicate the dependence of the capacity coefficient on inlet geometry in an almost directly proportional manner. It can be concluded that both the power and capacity coefficients behave similarly with a strong reliance on impeller inlet geometries, while insensitive to different suction piping configurations.

The significance of the hydraulic radius, r_h, for critical flowrates can be realized by explicitly analyzing the capacity coefficient. The flowrate is directly proportional to the average velocity and area, which in turn is proportional to r_h^2, substituting these into equation (5.12) we obtain:

$$\Pi_1 \propto \frac{\bar{V}}{Nr_h} \tag{5.17}$$

where Nr_h is known as the impeller peripheral velocity, U. When there is no prerotation (reverse flow), the tangent of the fluid inlet angle, β_f, is inversely proportional to the peripheral velocity. Therefore, relation (5.17) becomes:

$$\Pi_1 \propto \frac{\bar{V}}{U} \propto \tan \beta_f \ . \tag{5.18}$$

It is apparent from the above equations that when the hydraulic radius decreases the fluid incidence angle, $i=\beta_b - \beta_f$, increases. The angle of incidence is an influential parameter for the occurrence of reverse flow, and it depends on the fluid inlet angle. Therefore, the hydraulic radius controls the angle of incidence. When r_h is reduced,

"i" can be kept constant with reduced through flow, hence delaying the occurrence of recirculation.

It can generally be concluded that future studies involving recirculation should emphasize on the inlet characteristics of the pump, since it was repeatedly proven to be the most effective parameter affecting the pump critical flowrate and the power performance.

5.4 Inlet Flow Profile

a) Velocity Analysis:

To understand flow recirculation it is essential that we know the fluid behavior at the pump inlet. The pressure and velocity characteristics of the incoming flow should supply the necessary information needed to determine this behavior. The data obtained will also enable us to draw definite conclusions about the effects of the inlet flow on recirculation, and in turn the pump performance. The results previously obtained and discussed in this study will gain further significance and support with this new information.

The velocity was only monitored when the conical inlet guide vane was installed in the clear plexiglass pipe. The vane acting as a nozzle, increased the fluid velocity at the pipe wall periphery in order to suppress any tendencies of the flow to reverse. Since this was the most effective velocity technique in delaying the occurrence of recirculation, it was preferred over the others for our analysis. A five hole pitot probe was used to trace the flow velocity both vertically and horizontally at the section downstream of the vane. Pressure readings were taken at nine radial points for each flowrate

and were later converted into velocity terms. When the two lateral (side) holes had equal pressure values indicating that the probe was in line with the mainstream of the flow, the center hole provided the total stagnation pressure, P_t. By rotating the probe exactly 90 degrees from this point the corresponding static pressure, P_s, was obtained.

The approach used to convert the pressure readings into correct velocity values was a little tedious and is outlined below. Since both the total stagnation and static pressures were recorded at the same location, the Bernoulli equation was rearranged to be:

$$v^2 = \frac{2(P_t - P_s)}{\rho} \quad , \tag{5.19}$$

where v represents the local flow velocity. This value, however, needed to be corrected by a calibration correction factor, ε. Since the probe manufacturer did not supply a calibration chart for water tests and each individual probe needs to be calibrated, a special calibration test was devised. The probe was installed far upstream so that the readings would not be affected by the complex flow behavior at the pump inlet. The test was performed at a range of flowrates, and each recording was repeated and averaged for repeatability and to reduce data scatter.

Equation (5.19) had to be rearranged to determine the correction factor. If we divide both sides by the theoretical true velocity term u^2 and rearrange the u and v's, we obtain:

$$u = \left(\frac{2(P_t - P_s)}{\rho (v/u)^2} \right)^{1/2} . \qquad (5.20)$$

The $(v/u)^2$ term was designated as the correction factor, ε. With unit conversions at a temperature of 60°F, equation (5.20) becomes:

$$\varepsilon = \frac{148.5635 (P_t - P_s)}{u^2} \qquad (5.21)$$

where the pressure values are in psi and u, in feet per second is determined from the velocity profile equation of Fox and McDonald [33] for fully developed turbulent flow in a smooth pipe:

$$\frac{u}{U} = \left(1 - \frac{r}{R}\right)^{1/n} , \qquad (5.22)$$

where r is the local radial distance, R the pipe radius of 1.725 inches, and U the maximum velocity (at centerline). The turbulent behavior of the experimental flow range was determined from the calculated Reynolds number based on the average flow velocity, and the pump test code. The value of the exponent "n" depends on the Reynolds number, and for the flow range we were interested in, a value of 7 was determined to be appropriate. The U values were determined from:

$$U = \frac{\bar{v} (n+1)(2n+1)}{2n^2} , \qquad (5.23)$$

where $\bar{v}$ is the average velocity determined from the corresponding flowrate and pipe area in the form of:

$$\bar{v} = \frac{Q}{A} . \qquad (5.24)$$

The correction factors for each radial distance are plotted, and an average calibration curve produced in Fig. 51. Readings were not taken near the pipe wall, since they would be affected by the wall as indicated by Treaster [38].

Upon completing the calibration tests, the conical guide vane was installed in the pipe. It was placed at three different locations upstream of the probe in order to recreate the actual operating conditions of A, B, C as referred to in Chapter 4. The readings taken from the probe were therefore indicative of the impeller plane. Since we were interested in observing the velocity effects on recirculation, tests were performed at the low and high speed critical flowrates of each case. The flow was traced to record nine readings, and each test was repeated for accuracy. As a sample the original pressure measurements, the determined ε, u, and $(u/\bar{v})$ values at each radius are presented for both the high and low speed critical flowrates of case A in Appendix C.

The $(u/\bar{v})$ values for both flowrates of each case were averaged and the five locations constituting the top portion of the pipe are presented in Table 7 with their respective radii. The final plot of $(u/\bar{v})$ vs (r/R) is therefore obtained and shown together with the conical vane's leading and trailing edges in Fig. 52 for a range of zero (centerline) to R. Only the top portion of the velocity profile is given since it is expected to be symmetric about the pipe axis, however a slight asymmetry was noticed due to the minor construction imperfections of the vane. It can easily be seen that the vane distance from impeller plane does not alter the flow profile at the

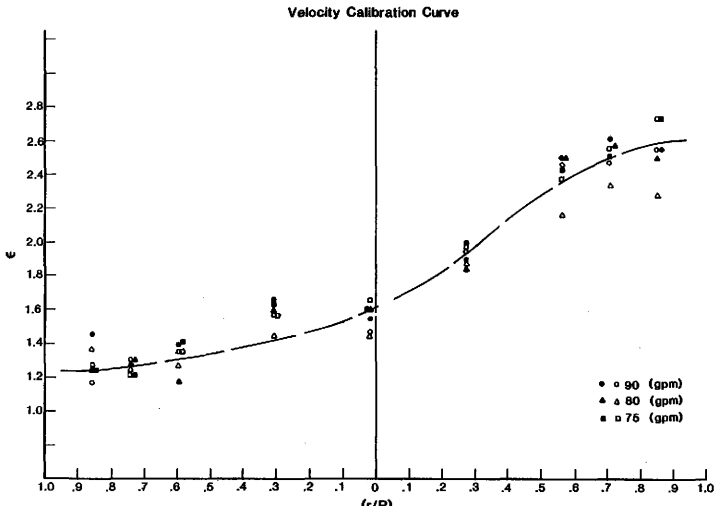

Figure 51. Velocity calibration curve.

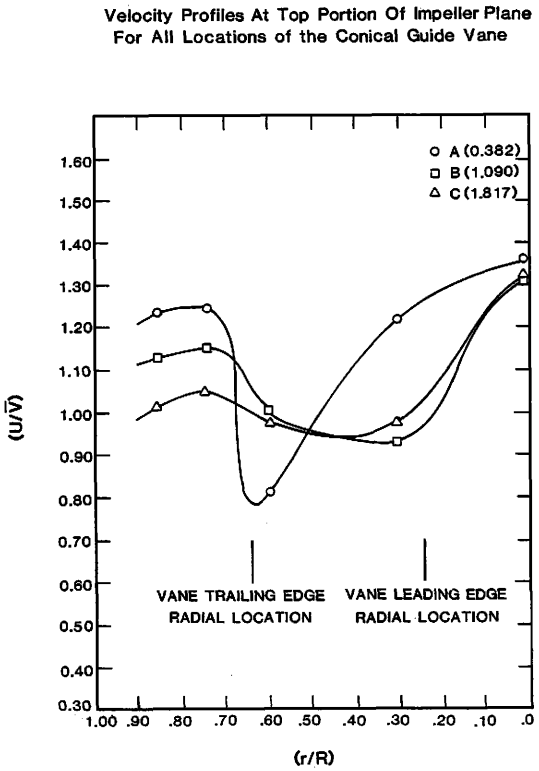

Figure 52. Velocity profiles at top portion of impeller plane for all three locations of the conical inlet guide vane.

Table 7. Flow velocity values at top portion of impeller cross-section for all cases of the conical inlet guide vane.

r/R	$(u/\bar{v})$		
	A	B	C
.8551	1.2356	1.1290	1.0166
.7391	1.2425	1.1500	1.0506
.5942	.8165	.9974	.9763
.3043	1.2167	.9268	.9756
.0145	1.3567	1.3067	1.3199

centerline, but as expected it causes a distinct velocity increase at the vicinity of the pipe wall. The sharp drop in curve A is due to the closeness of that experimental point to the vane trailing edge. Most importantly it can be concluded that as the vane is brought closer to the impeller plane a higher velocity at the impeller tips is achieved, contributing to the delay of the flow reversal. The above results indicate a direct relation between flow velocity at pipe wall and critical flowrates, and this can easily be observed from Table 8. An average velocity increase of 9% from case C to case A proves to be 8% more effective in delaying the onset of recirculation. By increasing the angle of inclination of the inlet vane further velocity improvements may be made, since this would enhance the vane's nozzle effect at the pipe wall.

b) Pressure Analysis.

In all experiments the suction pressures were recorded at three different inlet sections. The four circumferential readings at each

Table 8. Comparison of Impeller Tip Velocities with Their Respective Critical Flowrates for all Cases of the Conical Guide Vane

Vane Location	Low Speed		High Speed	
	U (fps)	Q_{cr} (gpm)	U (fps)	Q_{cr} (gpm)
Case A	2.5643	62.50	3.4797	79.30
Case B	2.4720	64.20	3.3509	84.60
Case C	2.3512	68.20	3.1271	86.10

section were used to determine the critical flowrates. These values were analyzed in a different manner to identify the inlet pressure behavior, which will complement the above results. The suction pressure values obtained at each flowrate were plotted with respect to their angular locations on the pipe. The resulting plots were indicative of the inlet wall static pressure distribution, and they provided very valuable information. A typical set of plots are presented in Figures 53 to 59. The most important observation common to all of these figures was that the angular static pressure distribution changed from an axisymmetric form to asymmetric when the flow was reduced beyond the critical value. The asymmetry reaches its peak at shutoff flow. At high deliveries the pump inlet pressures are lower than the upstream values due to wall friction losses, but at flowrates below the critical the inlet values are higher due to the intensity of the swirling reverse flow.

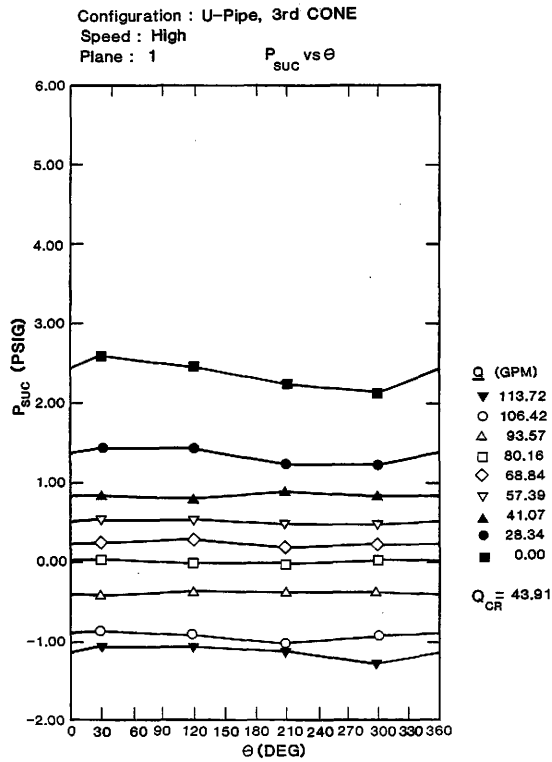

Figure 53. High speed first section circumferential pressure distribution for the U-pipe with third cone.

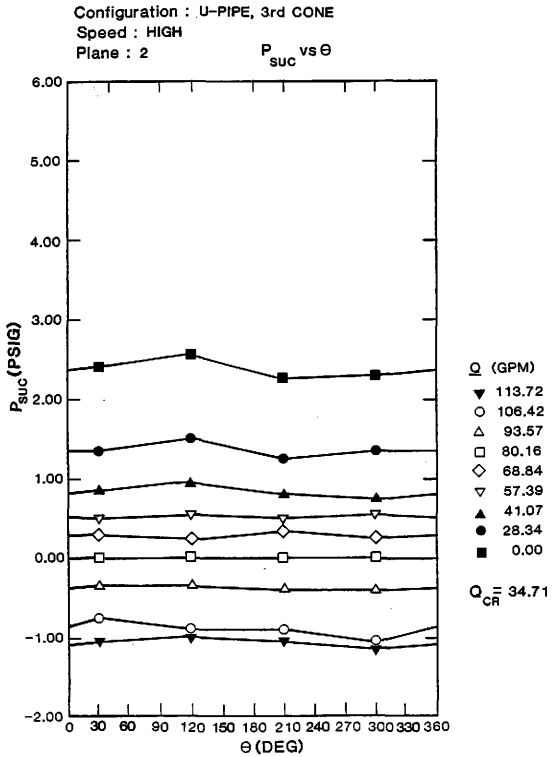

Figure 54. High speed second section circumferential pressure distribution for the U-pipe with third cone.

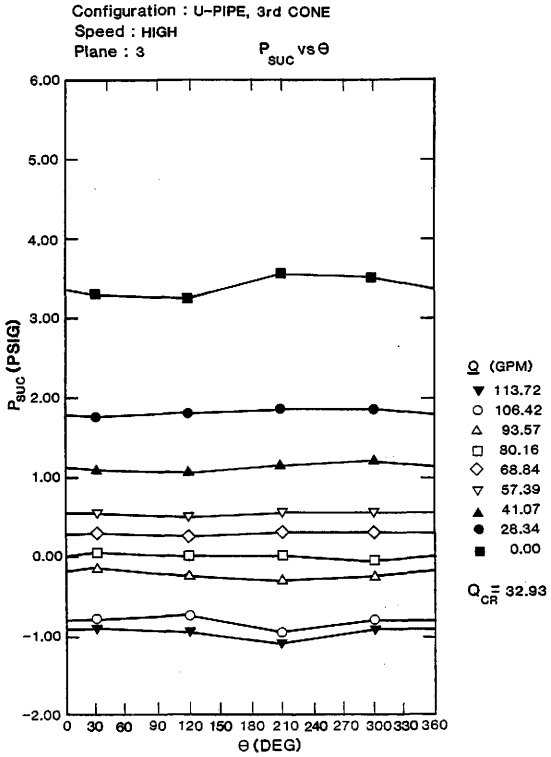

Figure 55. High speed third section circumferential pressure distribution for the U-pipe with third cone.

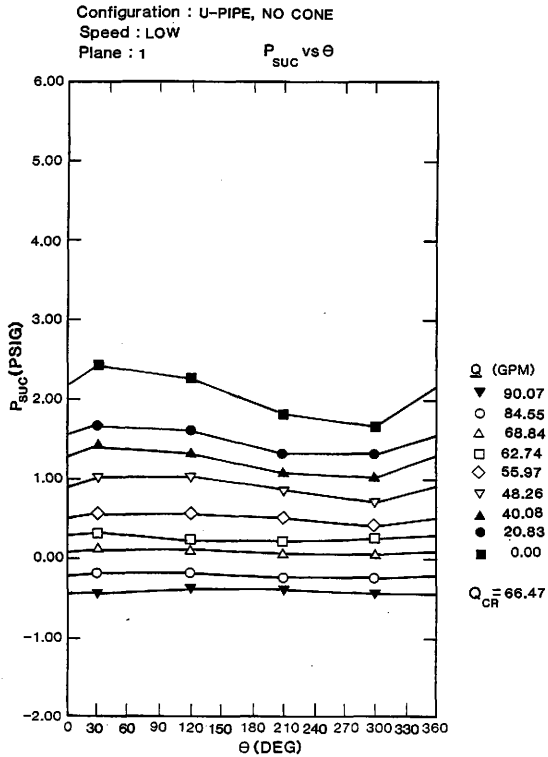

Figure 56. Low speed first section circumferential pressure distribution for the U-pipe.

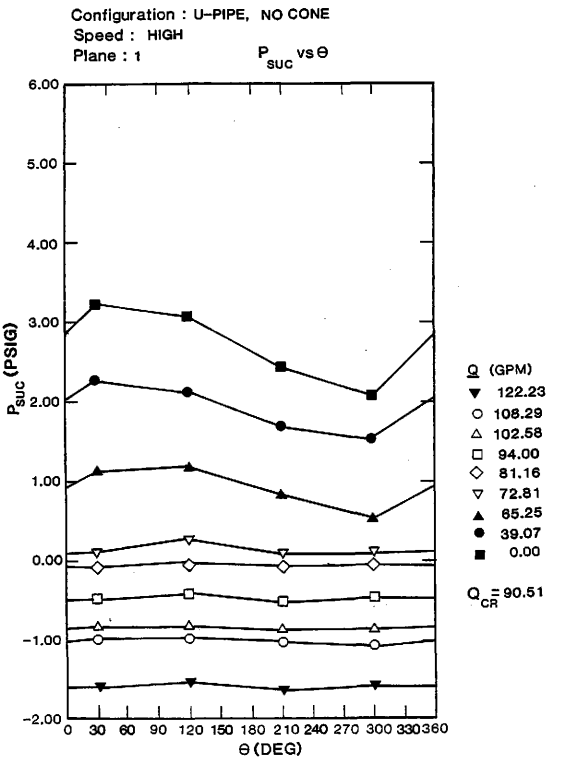

Figure 57. High speed first section circumferential pressure distribution for the U-pipe.

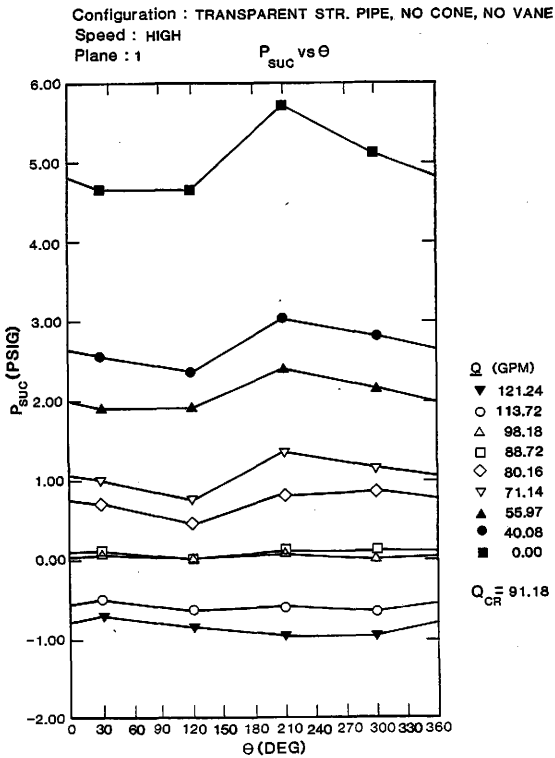

Figure 58. High speed first section circumferential pressure distribution for the straight pipe.

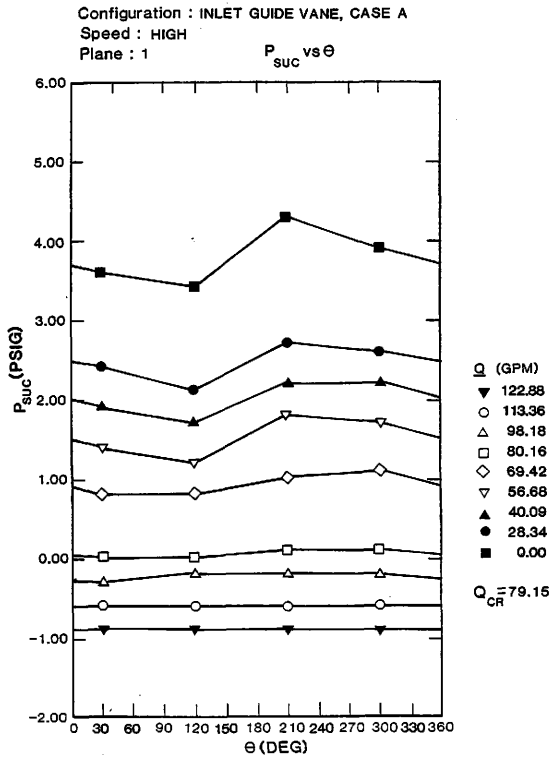

Figure 59. High speed first section circumferential pressure distribution for the straight pipe with conical guide vane (case A).

The first three figures belong to the case when the third cone is installed in the U-pipe, and the pump operating at high speed. Figure 53 shows the pressure distribution profile of the test section nearest to the impeller plane, while 54 and 55 show the other two upstream test section results. The asymmetry observed at low flows is due to the swirling character of the reverse flow. The pressure distributions of the first two sections are very similar both in form and magnitude, but the third most upstream section has a different distribution and higher values. This most probably is due to the interaction of the recirculating flow and the secondary flow caused by the elbow.

Figures 56 and 57 provide a comparison for the speed effects on inlet pressures. These figures are the results for the U-pipe, operating without any cones and values taken at the first section. It can easily be seen that the speed does not affect the form of the curves, but at high speeds the magnitudes change to result in a higher range of values. Since the cones do not interfere with the pipe wall they do not have any visible effects on the pressure profile. When all U-pipe pressure profiles are analyzed it is seen that there exists a high pressure region around 60 degrees, and a depression region at 300 degrees. Figure 58 can be compared with 57 to determine the effect of inlet piping on the pressure distribution, since both plots were obtained without a cone and at the same test section and speed. The wall static pressure values are higher at the first two test sections of the straight plexiglass pipe. Whereas, at the last section the U-pipe results are higher, and this rise may be attributed to the

secondary flows introduced by the elbow. These differences were expected since the U-shaped pipe was proven to be 6% more effective than the straight plexiglass pipe in delaying the inception of recirculation. The high and low pressure regions for the straight pipe seem to be out of phase with the U-pipe, indicating the dependency of the pressure distribution on the inlet piping.

Finally, from Figure 59, the effects of installing a conical inlet guide vane in the plexiglass pipe can be observed. Upon comparing figures 58 and 59 it can be seen that the vane does not alter the pressure variation trend, but slightly changes the magnitudes at the first test section. This change was expected since with the vane an 8% improvement was achieved. The different speeds show the same tendencies in the straight plexiglass pipe with and without the conical vane as in the U-shaped pipe. When performing high speed tests with the clear plexiglass pipe it was visually observed that the reverse flow reaches up to seven pipe diameters from the inlet plane at shutoff, while this number was five at low speeds. The intensity of recirculation and swirl gradually decay as the reverse flow progresses upstream and eventually disappears. Because of the short distance of the elbow from the impeller plane and due to the intensity of the swirling reverse flow, it is presumed that this flow goes beyond the 90 degree elbow.

5.5 Comparison of Results with Previous Study

In order to determine the accuracy and repeatability of the test data, and to see the effects of different critical flowrate determination techniques it was decided to numerically compare the results of

this study with Prince's [1]. Both studies were basically carried out with the same experimental setup, the only modification in this test was the addition of an extra lip seal to the pump to prevent the mixing of oil and water. Prince used the straight plexiglass pipe with and without the conical impeller covers, while these were used along with a U-shaped inlet pipe and three different inlet guide vanes in this study. In this experiment the test with the straight pipe without any cones performed by Prince was repeated and will help for comparison.

The most important change in this study was a different technique used to determine the various critical flowrates. As explained and discussed in Section 5.1 Prince used the "string" technique, while the "pressure" method was applied to this study. For the straight pipe repeated test the critical flowrates differed by 8 and 3% for the low and high speeds respectively. In both cases the previous study showed lower values, and it can be said that on the average the "string" technique results are 5.5% less than the "pressure." This difference could be acceptable for quick and rough estimates considering the amount of time and money saved with the "string" method, but the pressure technique will always yield more accurate and reliable results. From comparison the highest variation among the two techniques was observed to be 11%. When results of both inlet pipings were compared, the U-pipe had proven to be 6% more effective in delaying recirculation. However, when the U-pipe results were compared with Prince's straight pipe results this value dropped to 4.5%, the difference is attributed to the analyzing techniques.

If the input shaft power vs. flowrate curves of the original and repeated straight pipe tests are analyzed, it is observed that the recent study drew more power throughout the flow range, this increase can be explained with the addition of the lip seal.

The impeller covers were determined to be very effective in delaying recirculation at low flows, but they adversely affected the pump performance at high flowrates. Upon this observation it was decided to use the inlet conical guide vane, which as expected was proved to be favorable for the whole flow range, but not as effective as the covers at low flows. The power dissipated into the suction with recirculation and the critical flowrates were nondimensionally correlated and discussed for both studies in sections 5.2 and 5.3.

5.6 Comparison of Results with Proposed Theory

The additional power drawn by suction recirculation was designated as P_r, and discussed in Section 5.2. All this extra power is transported back into the inlet pipe with the reverse flow and eventually dissipated as heat. It would be beneficial for pump users and designers to have an analytical model to estimate the losses incurred by the inlet recirculation. Fraser [31] recently developed an analytical procedure to predict the onset of recirculation, but he was not concerned with the power aspect. However, in a recently published article Tuzon [32] proposes a method to calculate the recirculation power losses. By analyzing the flow entering the impeller he develops a formula to predict these losses and it is given as:

$$P_r = C \rho \frac{\omega^3}{2} \left[\frac{A}{\pi} \left(1 - \frac{Q}{Q_o}\right) \right]^{2.5} \qquad (5.25)$$

where Q_o is the pump design flowrate, A the pump inlet area and C a dimensionless correction factor reliant on the pump inlet geometry. Tuzon indicates that this equation provides a good basis for more accurate and refined analysis.

Following his suggestion a more refined approach was devised in order to take care of the ambiguity created by the nondimensional factor. The dimensionless shutoff power coefficient Π_3 was earlier correlated with the Reynolds number and then the through flow power coefficient was correlated with the flow coefficient. The later relation was correlated with equation (5.9). Substituting the definition of the power coefficient Π_3 given in equation (5.2) into (5.9), equation (5.10) was obtained as:

$$P_r = \Pi_3 \rho \omega^3 D_h^5 \left(1 - \frac{Q}{Q_o}\right)^n \qquad (5.10)$$

where D_h is the hydraulic diameter to be obtained from equation (5.6). For the whole flow range the slope of the best fit correlation straight line, n, was determined from Figure 49 to be 3.4, as opposed to 2.5 as suggested by Tuzon. The correlation coefficient being close to three confirms and supports the hypothesis that the recirculatory power behaves like a third order polynomial and is a primary factor for the input shaft power distribution. The experimental power loss values were presented in Table 5. Performing the necessary unit conversions and substitutions equation (5.10) became:

$$P_r = (3.6695 \times 10^{-9}) \Pi_3 N^3 \left(1 - \frac{Q}{Q_o}\right)^n \qquad (5.26)$$

Since our tests were performed at two different speeds, the above equation had to be modified separately for each speed. The normalized speeds of 5600 and 3800 were used respectively for the high and low speed tests. From equation (5.8) the corresponding Reynolds numbers were calculated and their respective Π_3 values were obtained from Figure 48. Errors due to a certain shutoff reading were diminished since the best fit line accounted for all the inlet geometry shutoff power loss values. Substituting the corresponding values of Π_3, N and Q_o, for both the high and low speeds equation (5.26) respectively becomes:

$$P_r = 1.3469 \left(1 - \frac{Q}{180}\right)^{3.4} \tag{5.27}$$

and,

$$P_r = .7410 \left(1 - \frac{Q}{122}\right)^{3.4} \tag{5.28}$$

where the Q values are in gpm and P_r in horsepower (Hp). To check the accuracy and for comparison purposes, Tuzon's proposed n value of 2.5 was also used in the above equations and plotted in Figures 60 and 61 respectively for the high and low speed cases. The respective experimental data obtained from both inlet pipings operating without a cone are also supplied in these figures.

From Figures 60 and 61 it can easily be realized that the "n" value determined from our Π vs $(1 - \phi)$ correlation results in a better estimate of the experimental data. This might have been expected since we specifically accounted for the flow inlet area and used a

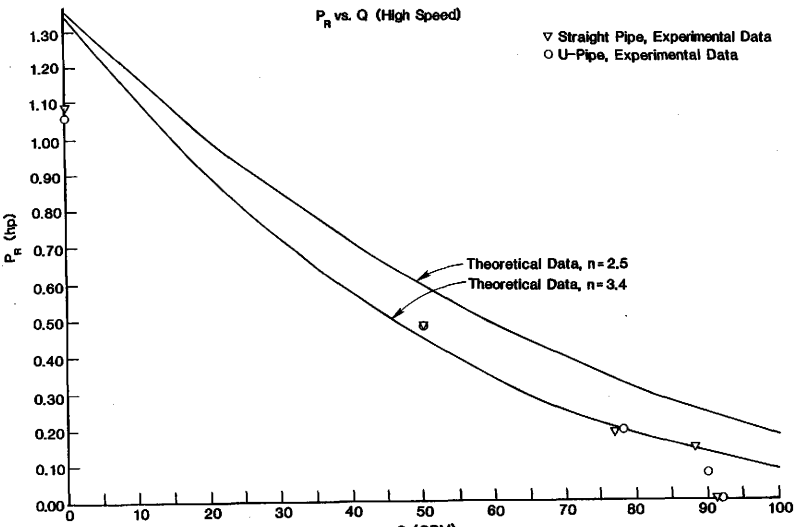

Figure 60. High speed comparison of experimental and theoretical power loss due to suction recirculation.

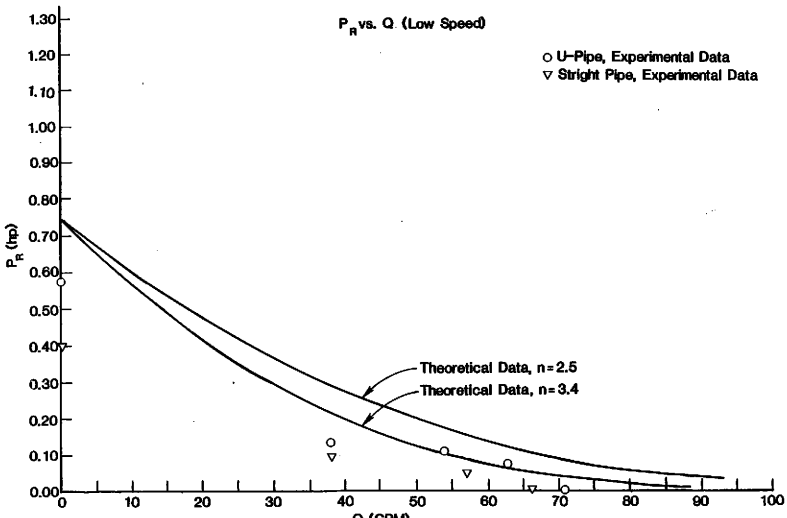

Figure 61. Low speed comparison of experimental and theoretical power loss due to suction recirculation.

determined pump parameter in our calculations. Further studies are needed to be carried out to determine an acceptable and reasonable "n" value for all pumps. The theoretical results compare better with the high speed experimental data due to the scatter of the low speed values around the best fit line of Figure 49. Even though high speed results are more accurate and reliable there seems to be a mismatch between the experimental and theoretical results at low flowrates. This can easily be verified from Figure 48, by noticing that the shutoff data points for the cases we are analyzing are slightly off the best fit line. This observation is strengthened with the low speed shutoff data taken from the straight pipe operating without any cones. This point deviates considerably from the best fit and results in a fairly poor agreement between the experimental and theoretical data. These results confirm the importance of the accuracy of the best fit line.

It is important to note that equation (5.10) is only valid from shutoff up to the point of critical recirculation. The experimentally determined critical flowrates are shown in Figure 60 and 61 on the horizontal axis which indicate zero recirculatory power loss. Equation (5.10) was tried with the critical flowrate replacing Q_o, but gave very poor results. Since Q_o is readily available and covers a fuller range of the flow it is accepted as appropriate. It is important to know the pump critical flowrate however, in order to estimate where the effectiveness of equation (5.10) terminates. These values were given in Table 3. If the shutoff power loss value for a certain case is available it might be substituted for $(\Pi_3 \rho \omega^3 b_h^5)$ in equation

(5.10) to give a fair estimate of the suction recirculation power loss up to the critical point.

It is believed that a significant contribution is made with this analysis, and further studies will support or modify the newly proposed method and results. The importance of the subject is apparent when considering that these power losses may account up to 30% of the total input power at shutoff conditions for the high specific speed axial-flow pumps.

CHAPTER VI. RECOMMENDATIONS AND CONCLUSIONS

6.1 Recommendations

The experimental research was carried out successfully with the aid of the available instrumentation. However, during the tests a few problems were confronted and in order to upgrade the test rig for future possible studies, some modifications are deemed necessary. These improvements and a few topics that should be studied are discussed in the next few sections.

a) Experimental apparatus

If it is desired to implement new studies on the existing setup, some changes are inevitable. The best efficiency point of the pump was never attained, this did not constitute any problems for the present study since we were mainly interested in the low flows. If a higher flow range is required the discharge piping might be modified by eliminating the flow resistant elbow and straightener. The flow after passing through the discharge valve and the orifice should be directly discharged into the tank.

At certain modes of operation the pump drew up to 4 horsepower, while the pump motor rating was 2.8 Hp. This caused overloading for this squirrel-cage induction type motor and in some instances prevented operation. If this motor was to be removed and the pump coupled with a 10 Hp external motor these problems would be avoided. With this modification there would also be no need for the generator, regulator and all the three phase wiring to go with it. If a generator is

still needed, then the existing generator should either be replaced or a better means of cooling should be provided, since it can become overheated in a short period of testing.

An automatic speed controller would definitely be preferred over the tedious process of changing pulleys every time a new speed is desired. The installation of a vacuum pump to extract air and gases entrapped in the system would provide more accurate and reliable data.

b) Measurement techniques

Even though the instrumentation employed in this study was sufficient, it could be upgraded for quick and accurate data acquisition. If the pump motor was to be removed, it could be replaced by a torque transducer which would enable easy power and speed determination. The rotational speed could also be obtained through the use of a fiber-optic proximity probe connected to a pulse counter (tachometer). With the correct speeds the precision of the calculations would be enhanced.

Each pressure measurement was made through the use of a pressure transducer, a carrier demodulator and a digital voltmeter. All three of these could be lumped into one, as it is done in Entran's EMP40 series. This would take less space, easier to calibrate, save time and increase accuracy, and is available in differential form.

The orifice plate was used for flowrate calculations. It is simple, economic and easy to install but has a high head loss which limits flow capacity. Accumulation of suspended matter at the inner side of the plate is possible, and may cause faulty readings. For

high flowrate applications and accuracy a venturi or a turbine flowmeter would be preferred.

After a thorough calibration, the five hole pitot probe provided good velocity data. Due to the wall boundary layer effects, data could not be obtained close to the pipe periphery. The probe being economic and easy to install also has some disadvantages, mainly the geometry of the probe support and tip create obstacles to the oncoming flow, affecting the velocity readings. The small openings are liable to blockage causing erroneous data. This still is a widely used velocity detection device, considering the visual requirements, complexity and price of the laser doppler anemometer. Hot wire anemometers may also be considered for usage at low velocities.

The data compilation and reduction could be made very easy and quick, if all raw data was to be transmitted to a computerized data acquisition system which is equipped with an analog to digital converter. The results would be digitally displayed and with an appropriate program test results would be readily available.

c) Future studies

With the experience and results of this study behind, and after completing an extensive literature survey, it would only be appropriate to suggest some future studies. From the survey it was observed that a good number of papers related to recirculation and cavitation were available. Some of them indicated the interdependency of these two problematic phenomena, but all failed to address it. As it is stressed by Acosta [39] the time has come to study this subject. The

results of such a study will aid pump designers and users immensely. To study this subject, an extensive flow visualization and measurement has to be undertaken. The existing pump has to be replaced with one of larger size. Inevitably more accurate Net Positive Suction Head (NPSH) measurements will have to be made, and the hydraulic loop has to be extensively modified. Since cavitation is identified with noise, a hydrophone such as the B&K type 8103 can be used together with a charge amplifier and a spectrum analyzer to detect the inception of cavitation and its characteristics. Pressure taps at the pump inlet, volute and discharge, transparent casing and piping, high speed cameras and other flow visualization techniques such as observing dye motion will all aid in understanding the complex flow behavior at the pump inlet.

Inlet area reduction is proven to be very effective in delaying the onset of recirculation, further studies involving this concept will add to the current understanding. The inlet of the fourth conical cover used in this study should be completely covered to prevent any flow from entering the impeller. Since data obtained from this cone served as a reference for calculations, the reliability of test results will be assured, especially of the third cone since it is most sensitive to error.

If the determination of the complex experimental velocity distribution of the recirculation zone is made possible, then deducing from the Euler equation and assuming axisymmetric flow, the power loss due to suction recirculation can be determined from

$$P_r = 2\ \pi\rho\omega \int_{r_i}^{r_o} r^2\ V_t V_a dr \quad . \tag{6.1}$$

where V_t and V_a are respectively the velocity components in the tangential and axial direction, while r_i and r_o are the inner and outer radii of the recirculation zone at the immediate upstream of the impeller plane.

Future studies involving various types of pumps will be necessary to verify and/or modify the equation developed for determining the recirculation power loss. A "n" value applicable to all pumps will set a good criteria for pump designers as well as users.

The selection of the ideal pump inlet geometry and design should be controlled by the specific study requirements, actual operating conditions and the financial constraints. These factors should be considered essential for the implementation of all above recommendations.

6.2 Conclusions

Some of the more important and relevant conclusions of this study are grouped and can be summarized as follows:

1) Results of two identical tests carried out separately by author and previous investigator were in good agreement, indicating good experimental repeatability. The "string" and "pressure" techniques used for critical flow determination were comparable, but the pressure technique was determined to be more reliable and accurate.

2) Decreasing the impeller inlet area effectively reduced the shaft power loss associated with suction recirculation, and this reduction further increased with decreasing flowrates. The slope of the power curve shifts from negative to positive as the inlet area is decreased. As higher speeds are attained, pump power consumption is increased. (Box and cross vanes are highly undesirable in power consumption aspect.)

Shutoff power loss vs. Reynolds number, through flow power loss vs. flow, critical flowrate vs. inlet geometry can all be correlated with a straight line on log-log scale indicating the significance of the hydraulic radius on recirculation power loss and on delaying the critical flowrates.

An equation was developed to theoretically determine power loss due to suction recirculation, it compared better with experimental data as opposed to the one proposed earlier. The equation was determined to be valid up to the critical flowrate. In axial-flow pumps power loss due to recirculation was determined to be a significant portion of the input power.

The power loss due to suction recirculation and critical flowrates are dependent on the impeller inlet geometry, rather than the inlet piping configuration.

3) The decrease of the inlet area causes a head drop at high flows, while it increases the head at low flows. This rise causes a slight improvement in efficiency at low capacities.

The best fit lines of the section critical flowrates have negative slopes, indicating that the strength of the swirling

recirculatory flow increases with decreasing flowrates. At shutoff it may progress upstream to seven pipe diameters, even passing through the elbow.

U-pipe is slightly better than the straight pipe in delaying the onset of recirculation, but the conical guide vane is slightly better than the U-pipe. Conical vane is the most effective vane design. It does not retard head performance at high flowrates. Effectiveness of conical vane in delaying recirculation is further increased by bringing it closer to the impeller plane. As the conical vane is brought closer to the impeller the velocity at the impeller tips is increased, suppressing any tendencies of the flow to reverse. Most effective delaying technique of all is again the inlet area reduction. For both speeds critical flowrates were initiated approximately at half of design flowrate.

The most significant inlet geometry parameter is the hydraulic radius. It controls the incidence angle and hence, reverse flow. As it is decreased, shaft power is saved and recirculation free operating range is increased.

4) When flow is decreased beyond the critical point, the inlet pressure distribution shifts from axisymmetric to asymmetric. As flow is decreased further, the asymmetry increases due to swirling reverse flow and reaches a maximum at shutoff. At high flowrates, pump inlet pressures are lower than upstream values, but beyond critical it becomes vice versa. Secondary flows created by the U-pipe's elbow affect the inlet pressure

distribution. Speed does not alter form of distribution, but results in a higher range of values. Inlet pressure distribution is dependent on inlet piping, but it does not affect recirculation.

REFERENCES

1. Prince, T., "Suction Recirculation and Its Effects Upon Axial-Flow Pump Power Consumption," Master of Science Thesis," Texas A&M University, August 1983.

2. Toyokura, T., and Kubota, N., "Studies on Backflow Mechanism of Turbomachines. Part 1: Backflow on the Suction Side of Axial-Flow Impeller Blades," Bull. of JSME, Vol. 11, No. 43, 1968.

3. Baysal, K. and Ediş, K., "Santrifüj ve eksenel tulumbaların girişindeki ön-dönme olayının etüdü ve ön-dönmenin giderilerek tulumbaların geliştirilmesi yolları" TÜBİTAK, Proje No. MAG-219, 1976.

4. Tanaka, T., "An Experimental Study of Backflow Phenomena in a High Specific Speed Propeller Pump." ASME Paper No. 80-FE-6.

5. Javur, M., Murthy, K., and Kar, S., "Analysis of Performance Characteristics of Axial-Flow Pumps" ASME FED-Vol. 6, Nov. 1983.

6. Murakami, M., and Heya, N., "Improvement of Pump Performance by Impeller Eye Throttling." ASME paper No. 69-FE-26.

7. Peck, J. "Investigations Concerning Flow Conditions in a Centrifugal Pump, and the Effect of Blade Loading on Head Slip." Proc. I. Mech. E. Vol. 162, p. 409, Nov. 1950.

8. Okamura, T. and Miyashiro, H. "Cavitation in Centrifugal Pumps Operating at Low Capacities." ASME Polyphase Flow in Turbomachines Dec. 1978.

9. Howard, J., and Kittmer, C. "Measured Passage Velocities in a Radial Impeller with Shrouded and Unshrouded Configurations." ASME Paper 74-GT-66.

10. Lennemann, E. and Howard, J. "Unsteady Flow Phenomena in Rotating Centrifugal Impeller Passages." Journal of Engineering for Power, p. 65, Jan. 1970.

11. Yadav, R. and Yahya, S. "Flow Visualization Studies and the Effect of Tongue Area on the Performance of Volute Casings of Centrifugal Machines," Jr. Mech. Sci. Vol. 22 pp 651-660, 1980.

12. Minami, S., Kawaguchi, K., and Homma, T. "Experimental Study on Cavitation in Centrifugal Pump Impellers." Bull. of JSME, Vol. 3, No. 9, 1960.

13. Barrand, J., Caignaert, G., Canavelis, R. and Guiton, P. "Experimental Determination of the Reverse Flow Onset in a Centrifugal Impeller." Proc. of 1st International Pump Symposium, Texas A&M University, May 1984.

14. Breugelmans, F. and Şen, M. "Prerotation and Fluid Recirculation in the Suction Pipe of Centrifugal Pumps." Proc. of 11th Annual Turbomachinery Symposium, Texas A&M University, Dec. 1982.

15. Murakami, M. and Heya, N. "Swirling Flow in Suction Pipe of Centrifugal Pumps. First Report: Distribution of Velocity and Energy." Bull. JSME, Vol. 9, No. 34, 1966.

16. Schiavello, B., and Janigro, A. "Off Design Performance of Pumps, Prerotation in Centrifugal Pumps--Design Criteria." VKI LS 1978-3 March 1978.

17. Sen, M. "Off-Design Performance, Prerotation in Centrifugal Pumps," VKI LS 1978-3 , March 1978.

18. Toyokura, T. and Kubota, N., "Studies on Backflow Mechanism of Turbomachines. Part 2: Backflow to the Suction Side of Mixed-Flow Impeller Blades." Bull. JSME Vol. 12, No. 50, 1969.

19. Stepanoff, A., "Centrifugal and Axial Flow Pumps," New York, Wiley, 1957.

20. Oshima, M., "Inlet Flow and Aspects of Cavitation in Centrifugal Impellers." Proc. of 11th Annual Turbomachinery Symposium, Texas A&M University, Dec. 1982.

21. Sloteman, D., Cooper P. and Dussord, J. "Control of Backflow at the Inlets of Centrifugal Pumps and Inducers." Proc. of 1st International Pump Symposium, Texas A&M University, May 1984.

22. Karassik, I. "Centrifugal Pumps and System Hydraulics." Chemical Engineering, Oct. 4, 1982.

23. Schweiger, F. "Energy Conditions in Centrifugal Pumps at Low Flow." ASME FED-Vol. 6, Nov. 1983.

24. Fraser, W. "Flow Recirculation in Centrifugal Pumps." Proc. of 10th Annual Turbomachinery Symposium, Texas A&M University, Dec. 1981.

25. Şen, M. and Breugelmans, F. "Reverse Flow, Prerotation and Unsteady Flow in Centrifugal Pumps." Fluid Mechanics Silver Jubilee Conference Paper 3.1, Nov., 1979.

26. Schiavello, B. and Şen, M. "On the Prediction of the Reverse Flow Onset at the Centrifugal Pump Inlet." 22nd Annual Fluids Engineering Conference, March 1980.

27. Nelson, E. "Maintenance and Troubleshooting of Single-stage Centrifugal Pumps." Proc. of 1st International Pump Symposium, Texas A&M University, May 1982.

28. Morton, T., and Olin G. "Realistic Design Specifications Increase Pump Reliability." Proc. of 10th Annual Turbomachinery Symposium, Texas A&M University, Dec. 1981.

29. Murai, H., and Terauchi, H. "Observations of Cavitations and their Application for Analysis of Flow Patterns in Axial-Flow Pump at Partial Discharge." ASME Paper No. 73-FE-11, 1973.

30. Murakami, M., Heya, N. "Swirling Flow on Suction Pipe of Centrifugal Pumps. Third Report: Effect of Bend in Pipe." Bull. JSME Vol. 9, No. 34, 1966.

31. Fraser, W. "Recirculation in Centrifugal Pumps." World Pumps, May 1982.

32. Tuzon, J. "Inlet Recirculation in Centrifugal Pumps." ASME FED-Vol. 6, Nov. 1983.

33. Fox, R., and McDonald, A. "Introduction to Fluid Mechanics." Toronto, Wiley, 1978.

34. Shepherd, D. "Principles of Turbomachinery." New York, Macmillan, 1976.

35. "Application of Fluid Meters: Part II." Sixth ed., 1971. Report of ASME Committee on Fluid Meters.

36. "Flowmeter Computation Handbook." ASME Research Committee on Fluid Meters, 1961.

37. Mann, R., and Marston, C. "Friction Drag on Bladed Disks in Housings as a Function of Reynolds Number, Axial and Radial Clearance, and Blade Aspect Ratio and Solidity." ASME Journal of Basic Engineering, Dec. 1961.

38. Treaster, A. and Yocum, A. "The Calibration and Application of Five-Hole Probes." ISA Transactions, Vol. 18, No. 3, 1979.

39. Acosta, A. "Cavitation." Pump Short Course, Texas A&M University, May 1983.

APPENDIX A

DETAIL DRAWINGS

The first two figures depict the power measuring circuits used respectively with the low and high operating speeds. A 3000 and a 1500 wattmeter were used at the low speed, while three 3000 wattmeter were used with the high speed. The two different configurations were used in order to accurately cover the whole power range. The third diagram represents the actual wattmeter setup used during the calibration and testing.

Both portions of the cone mold are given with their dimensions in Figures 65 and 66. After installing these two aluminum parts the mixture of epoxy resin and hardener is poured. The fabricated cones are then machined for different frustrum heights.

In order to mount the conical impeller covers at the pump inlet, the pump inner housing required modification. Mounting brackets were installed on the housing and are shown together in Figure 67.

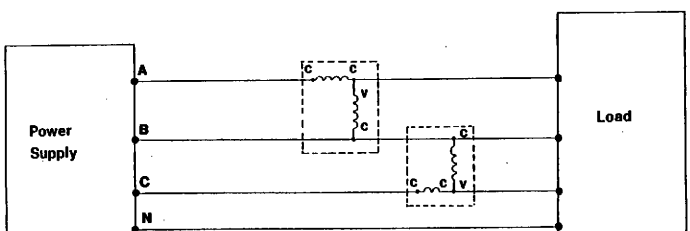

Figure 62. Low speed power measurement circuit.

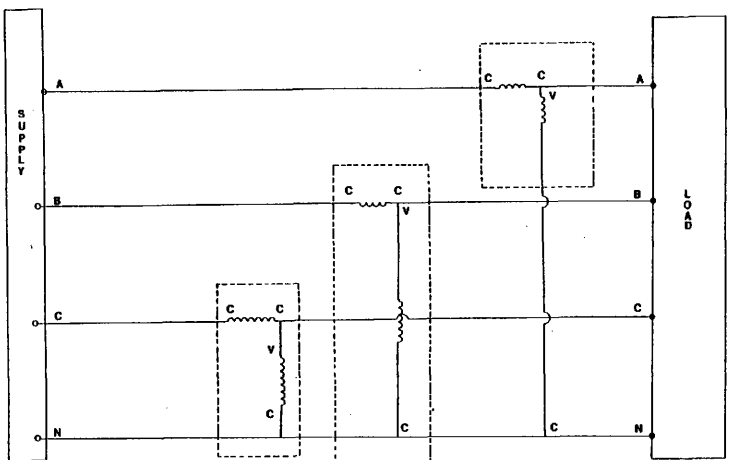

Figure 63. High speed power measurement circuit.

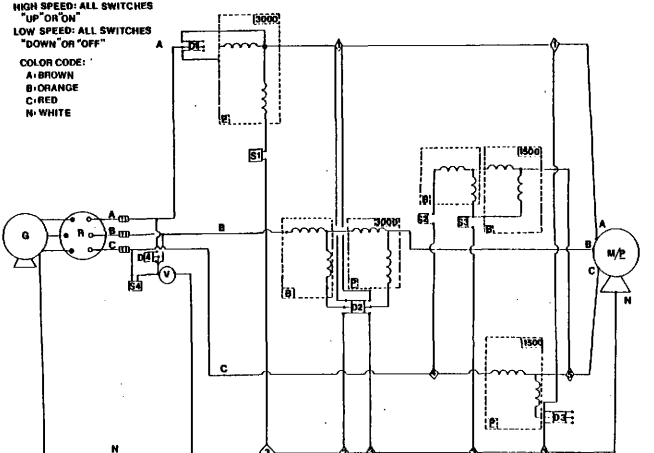

Figure 64. Detailed power circuit calibration diagram.

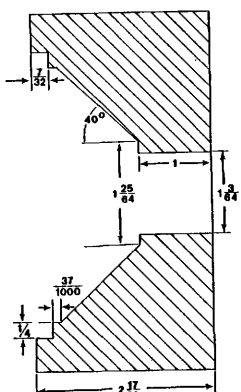

VIEW A-A

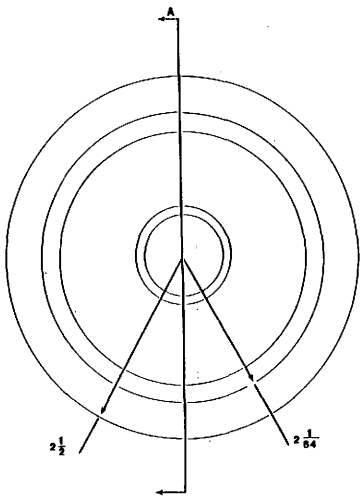

TOP VIEW

Figure 65. Female portion of cone mold.

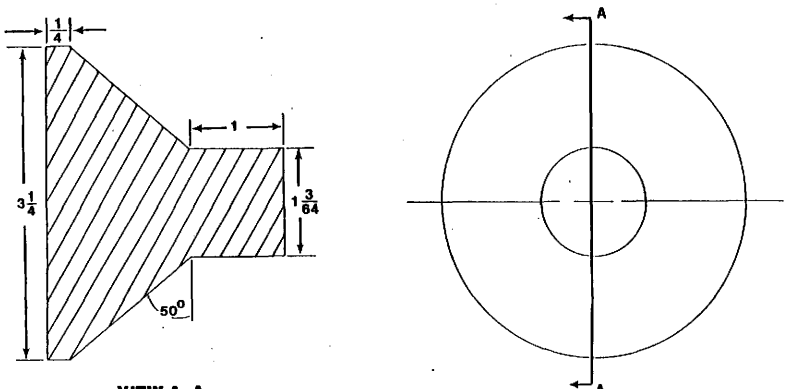

Figure 66. Male portion of cone mold.

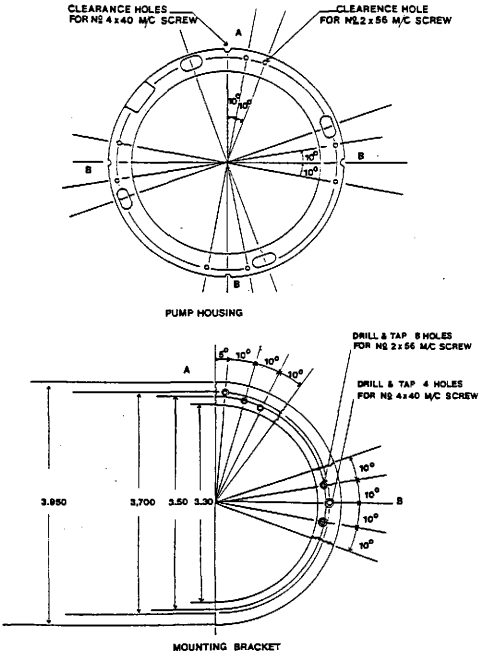

Figure 67. Cone mounting bracket and impeller housing.

APPENDIX B

METHOD FOR INPUT SHAFT POWER DETERMINATION

Input shaft powers for the high speed tests were obtained from a manufacturer supplied graph depicting true input power versus shaft power (Fig. 68). The actual input powers were determined as described in Section 4 of this chapter. Since there were no manufacturers' data available for low speed shaft powers, a slightly more complex approach was devised and applied. The dimensionless motor efficiency and the motor slip defined as

$$S = \frac{N_S - N}{N_S} \tag{B.1}$$

are employed as the primary parameters. Here N is the actual motor rotational speed and N_S is the synchronous speed found from

$$N_S = 120 \, (f \div p) \tag{B.2}$$

where f is the supply frequency and p the number of poles, which in our case is eight. A synchronous speed of 4170 rpm is calculated for low speeds, while this reaches 6000 rpm's for high speeds.

It is assumed that the functional relationship of slip versus efficiency plot obtained for the high speed case as shown in Fig. 69 is also applicable to the low speed case. This approach was also adopted and utilized by Prince [1]. To facilitate computations he fitted two straight lines to the data and derived their equations. The equations and the motor slip ranges that they apply to are given below:

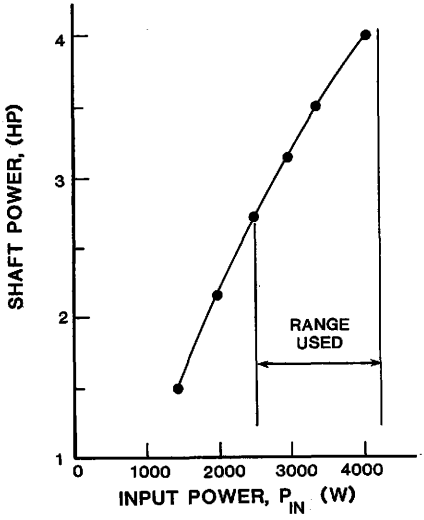

Figure 68. Shaft power vs. input power.

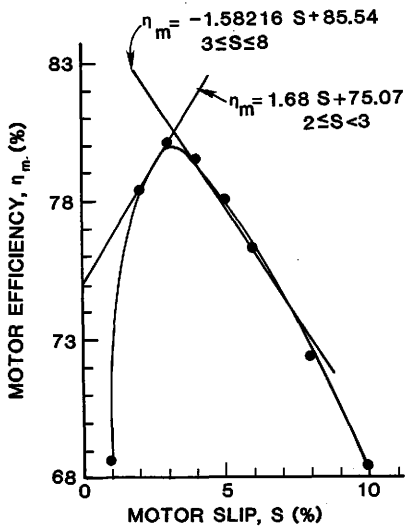

Figure 69. Motor efficiency as a function of motor slip.

$$\eta_m = 1.68S + 75.07, \quad 2 \leq S \leq 3 \tag{B.3}$$

$$\eta_m = -1.58216\ S + 85.54, \quad 3 \leq S \leq 8\ . \tag{B.4}$$

Both the efficiency and slip values are given as percentages.

The low speed shaft power determination was carried out in the following manner: first the panel meter power readings were converted to their actual values through equations (4.12) and (4.13). The rotational speed N was calculated from this power by equation (4.15), and substituted into equation (B.1) to give us motor slip. The motor efficiencies were found from either of equations (B.3) or (B.4). Finally, the true input power was multiplied with the motor efficiency to give the shaft power as,

$$P_{sh} = C(P_{in} \times \eta_m) \tag{B.5}$$

where C is a conversion coefficient.

Power loss due to recirculation constitutes a main portion of this study. Any minor errors incurred by the input shaft power calculations will be compensated for when determining the recirculatory power loss.

Table 9. Data for Case A of the Conical Inlet Guide Vane at Both Low and High Speed Critical Flowrates

		Q_{cr}(High) = 79.3 GPM $\bar{v}$ = 2.72 fps, U = 3.33 fps			Q_{cr}(Low) = 62.5 GPM $\bar{v}$ = 2.14 fps, U = 2.62 fps		
r/R	$(v/u)^2$	P_t-P_s (psi)	u (fps)	$u/\bar{v}$	P_t-P_s (psi)	u (fps)	$u/\bar{v}$
.8551	1.2933	.103	3.4397	1.2662	.058	2.5812	1.2050
.7391	1.2592	.105	3.5197	1.2957	.055	2.5474	1.1892
.5942	1.3292	.048	2.3162	.8526	.025	1.6716	.7804
.3043	1.5802	.115	3.2881	1.2104	.073	2.6198	1.2230
.0145	1.5565	.148	3.7585	1.3836	.085	2.8483	1.3297

VITA

Kenan Alpan was born on July 4, 1960 in Ankara, Turkey. He completed his elementary, secondary and high school education at Ankara College, graduating in 1977. He enrolled at Texas A&M University in the fall of 1977 and graduated in December 1981 with a Bachelor of Science degree in Mechanical Engineering. His permanent address is:

166 East 34th Street, #12D
New York, New York 10016